Final Technical Report, 2006

PEM Fuel Cell Freeze Durability and Cold Start Project

Report Date: May 31, 2007

Reporting Period: May 1, 2006 to April 30, 2007

Tim Patterson (primary contact), Jonathan O'Neill and Michael Perry
UTC Power (formerly UTC Fuel Cells)
195 Governor's Highway
South Windsor, Connecticut 06074
Tel: 860-727-2274, E-mail: *Timothy.Patterson@UTCPower.com*

Pat Hagans, Cindy York, and Rachid Zaffou
United Technologies Research Center
411 Silver Lane
East Hartford, CT 06108
(860) 610-7000

DOE Technology Development Manager: Kathi Epping
DOE Project Officer: Jill Gruber, Golden Field Office, 1617 Cole Blvd. Golden, CO 80401-3305 jill.gruber@go.doe.gov

Contract Number: ***DE-FG36-06GO86042***

Start Date: May 1, 2006

End Date: April 30, 2007

Objectives

UTC has taken advantage of the unique water management opportunities inherent in micro-porous bipolar-plates to improve the cold-start performance of its polymer electrolyte fuel cells (PEFC). Diagnostic experiments were used to determine the limiting factors in micro-porous plate PEFC freeze performance and the causes of any performance decay. Alternative cell materials were evaluated for their freeze performance. Freeze-thaw cycling was also performed to determine micro-porous plate PEFC survivability. Data from these experiments has formed the basis for continuing development of advanced materials capable of supporting DOE's cold-start and durability objectives.

Technical Barriers

- Barriers addressed
  - Start-up and shut-down time and energy
  - Water transport within the stack
  - Durability
- Targets
  - Unassisted Cold-Start: 50% rated power in 30 s from -30ºC
  - Survivability: 100 freeze-thaw cycles to -40ºC without decay

Accomplishments

Introduction

Traditionally, PEFCs use solid bipolar plates as an electronic interconnect and gas-tight seal between adjacent cells. Bipolar plates also contain flow-fields for air, fuel, and coolant. Since water generated at the cathode must be removed by the air stream, liquid water accumulates in the air flow-field and cathode gas diffusion layers (GDL). Moreover, the fuel must be humidified to prevent anode dry-out due to osmotic drag.

UTC has largely overcome these barriers by using micro-porous bipolar plates, which are permeable to liquid water but have a high bubble pressure. These water-transport plates (WTP) humidify the anode and remove excess liquid water from the cathode. The reactant gases need not be humidified, and the cells may be operated at atmospheric exhaust pressure, and low reactant pressure drop.

This work is concerned with the performance of micro-porous plate PEFCs under freezing conditions. For use in the automotive industry, PEFCs must be able to start from below-freezing temperatures within a short time. DOE's requirement, established in discussions with the auto industry, is 50% rated power in 30 s from -20ºC. To minimize start-up and shut-down time and energy, a cold start should be unassisted. The PEFC stack should be thawed using waste heat from the fuel cell reaction, without any external heating. An unassisted cold start is referred to as a "Boot-Strap Start" (BSS).

In UTC's baseline micro-porous plate short-stack, frozen cell resistance was much higher on the anode side than on the cathode side of the stack. The anode side of the stack is defined as the side in which the anode is towards the end of the stack, and the cathode is towards the middle of the stack, and vice versa for the cathode side. Similarly, the BSS performance of cells on the anode side of the stack was much worse than cells on the

cathode side of the stack. This anode-side performance decay was partially recovered by high current density operation and mostly recovered by running the cells in a hydrogen-pump mode (i.e., anodic oxidization of hydrogen on one electrode and cathodic evolution of hydrogen on the opposite electrode). Water movement during freeze, or frost-heave, was proposed as the mechanism of anode-side BSS decay.

Three strategies were employed to mitigate frost-heave and its effects, thereby lowering anode-side resistance increase and improving anode-side BSS performance. First, the baseline membrane electrode assembly, herein called MEA A, was compared to an alternative MEA, herein called MEA B, containing a more effective pore structure. MEA B was tested at both the sub-scale and the short-stack level. Second, the baseline gas-diffusion layers (GDL) were compared to various GDLs that are less permeable to liquid water. Low permeability GDLs were evaluated at both the single-cell and short-stack level. Third, cell configurations were compared with less water and, therefore, lower thermal mass. The low thermal mass cells were investigated at the single-cell level. Although all three strategies led to improvements in BSS performance, the MEA and GDL developments were most effective. Baseline MEAs and GDLs, as well as MEA B and low permeability GDLs, were all subjected to -40°C freeze-thaw cycling at the short-stack level and showed negligible freeze-thaw related decay after 100 cycles.

Results

Cold Start Performance of Baseline Cell Configuration

A 30-cell stack, with UTCs baseline micro-porous plate cell configuration, was built and tested for BSS performance. It was repeatedly frozen, started from various temperatures between -10°C and -35°C (Figure 1), allowed to warm itself up to 65°C with its own internally-generated heat, and operated for some time at various current densities before being re-frozen. To minimize shut-down energy, little or no active purging was performed before freezing. When frozen, the stack was allowed to soak for at least eight hours at the desired temperature (for example, -35°C). Stoichiometries during BSS were 2 for fuel and 3.33 for air. Investigation of the frozen cell resistances and cell-by-cell BSS performance revealed significant differences between the anode and cathode sides of the 30-cell stack. The frozen cell resistance was much higher on the anode side than on the cathode side of the stack, and increased with the rate of freeze. Similarly, anode-side BSS performance was much worse than cathode-side BSS performance. Figure 2 shows the voltage response during a 0.4 A/cm^2 start from –12ºC, and the cell resistances at –10ºC.

Two non-invasive methods were used to recover the anode-end performance loss. First, the stack was operated at high current densities (up to 1.6 A/cm^2). Such operation generates significant of heat in the cathode catalyst layer (CCL), thereby evaporating more water from the CCL. Figure 3 shows that a portion of the performance was recovered by this method. More effective than high current density operation was the use of hydrogen pumping (Figure 4 and 5). In this technique, hydrogen was fed to both electrodes, and a power supply was used to oxidize hydrogen on the cathode and evolve

hydrogen on the anode. The performance degradation of the anode end cells was nearly eliminated by the hydrogen pump. It is thought that the hydrogen pump recovers the performance by removing water from the CCL due to electro-osmotic drag. The recovery by hydrogen pumping (and to some extent, by high current density operation) demonstrates that the anode-side performance decay was mainly caused by CCL flooding.

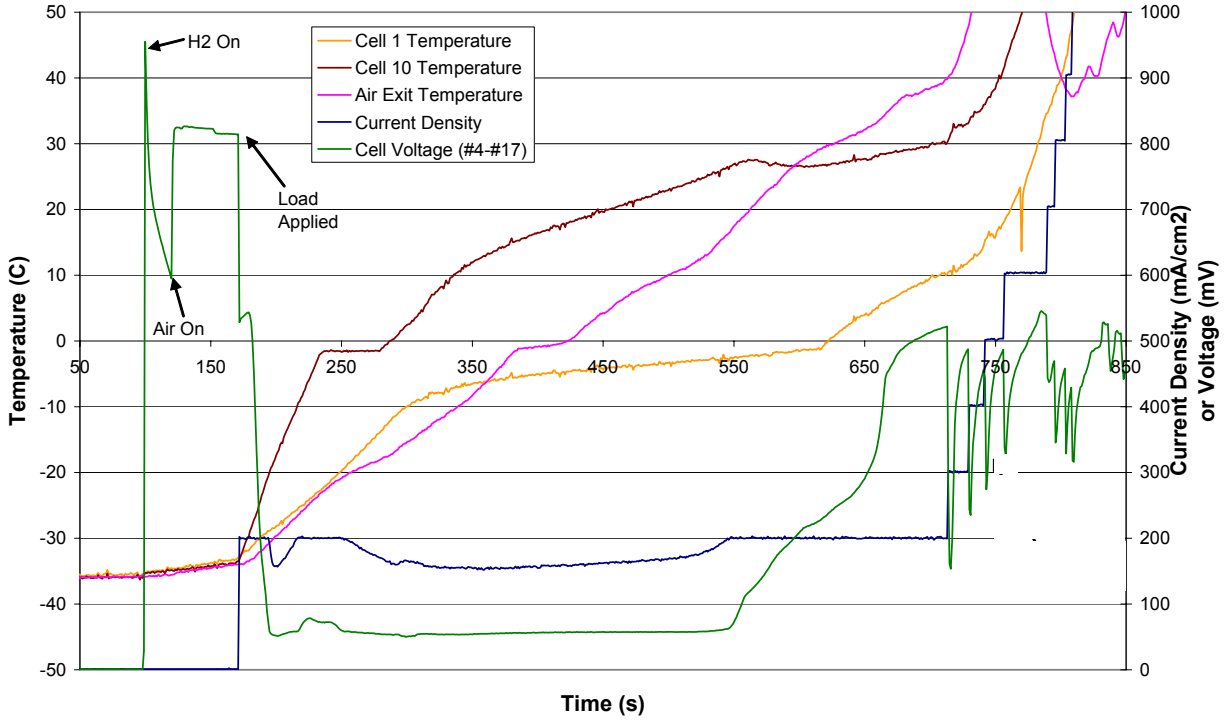

Figure 1. Baseline short-stack BSS from -35°C with no air-side purge and a short fuel-side purge for system components (e.g., fuel regulator).

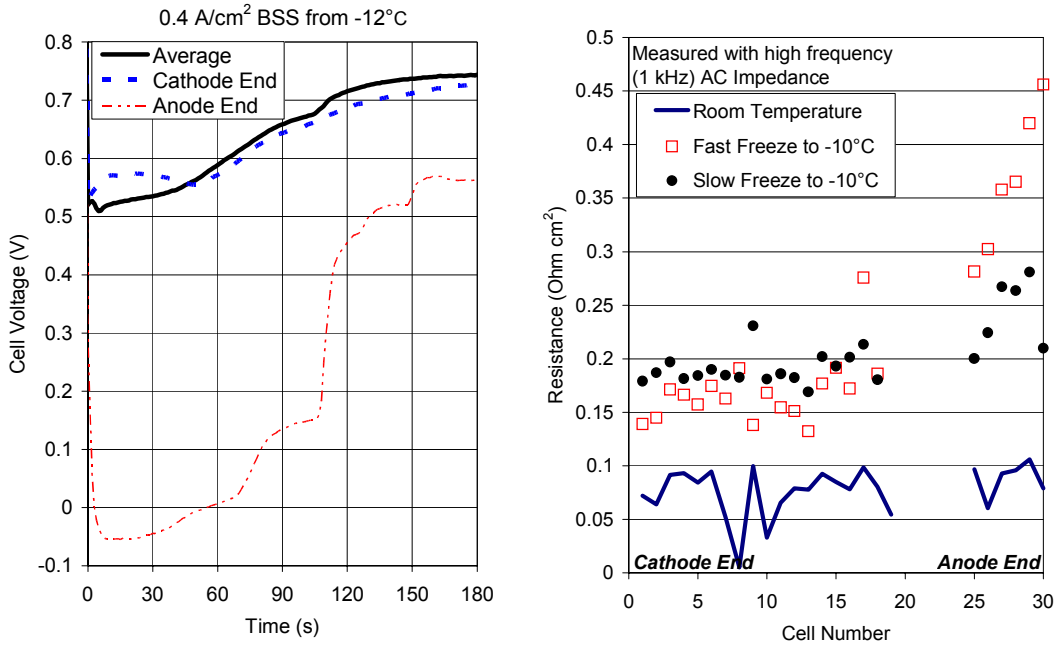

Figure 2. Effect of location in stack on freeze start-up performance and ohmic resistance.

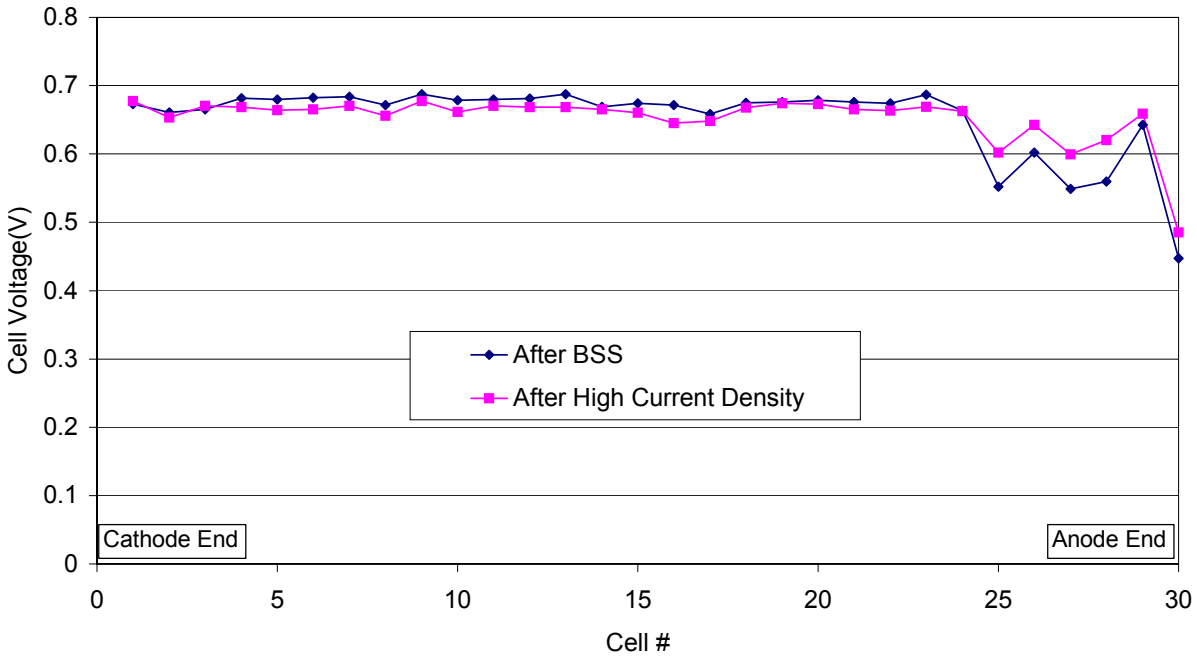

Figure 3. Cell voltages at 1 A/cm^2 before and after high current density (1.6 A/cm^2) operation. Fuel stoichiometry = 1.25; Air stoichiometry = 1.67.

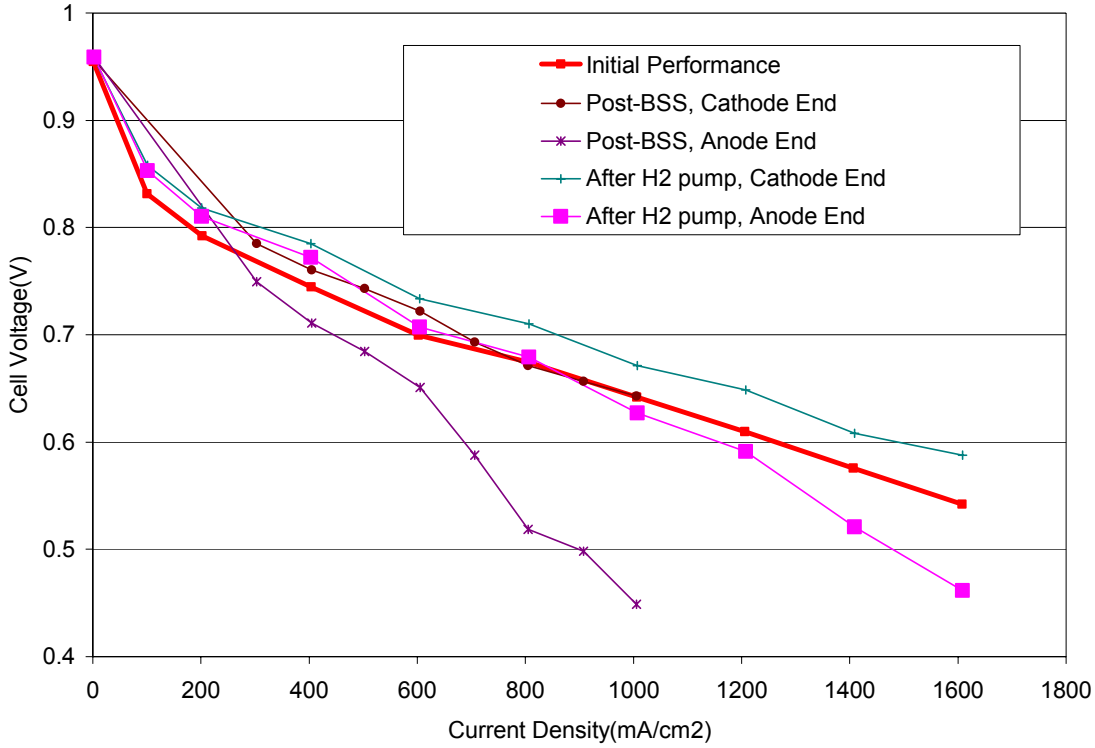

Figure 4. Polarization curves, before and after hydrogen-pump procedure.

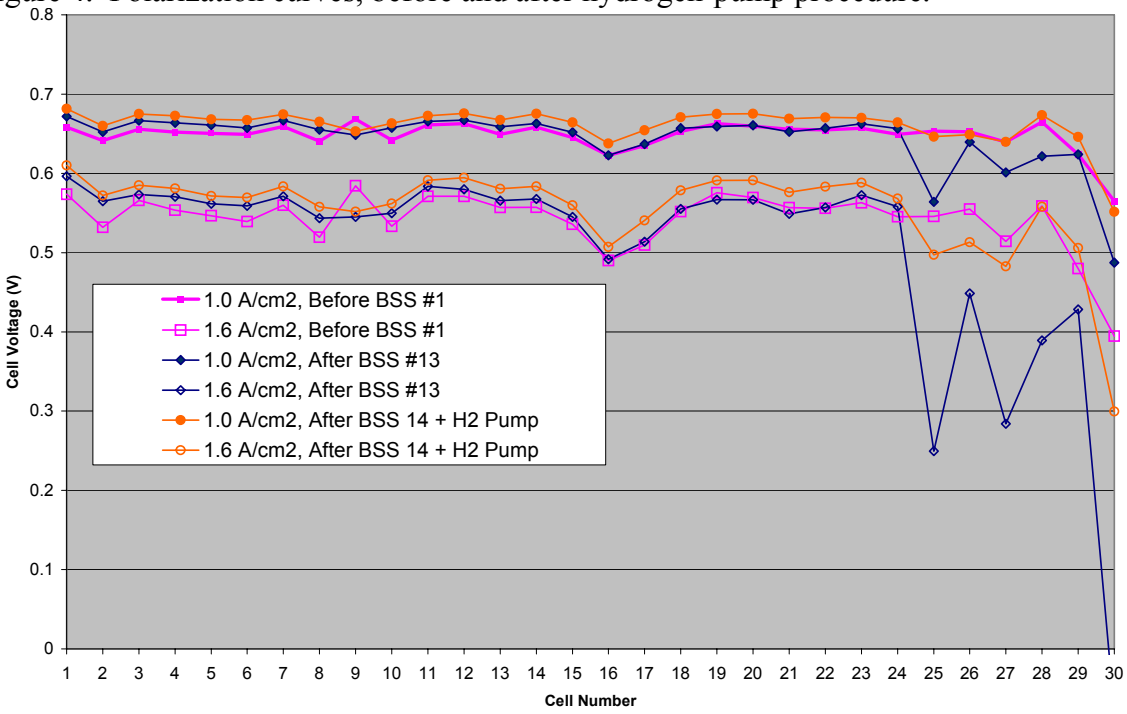

Figure 5. Performance vs. Cell Position: before BSS, after BSS, and after recovery by hydrogen pumping.

Mechanism of Performance Loss

It is hypothesized that water moves into the CCL due to a pressure gradient created by freezing in the small pores of the CCL. As this water freezes, the effective pore radius decreases, as shown in Figure 6. According to the following relation:

$$P_{gas} - P_{liq} = P_c = \frac{2\gamma \cos\theta}{r}$$

where P_c represents capillary pressure, γ represents surface tension, θ represents contact angle, and r represents radius, the liquid pressure decreases as the effective pore radius decreases at constant (atmospheric) gas pressure. The lower liquid pressure in a freezing pore causes water in other pores to move down a pressure gradient (which corresponds in this case to the thermal gradient), towards the freezing region. This phenomenon is known as "frost-heave," because in extreme cases, the excess of ice which is formed in a small region may deform the surrounding medium.

Because water tends to move down its thermal gradient by means of the frost-heave mechanism, water should move in different directions on opposite sides of the stack, as depicted in Figure 7. On the cathode end, water should move out of the CCL, across the cathode GDL, and into the cathode WTP. On the anode end, water should move from the cathode GDL into the CCL, thus increasing mass transport losses in the CCL, while the formation of an ice lens between the GDL and CCL may result in increased contact resistance.

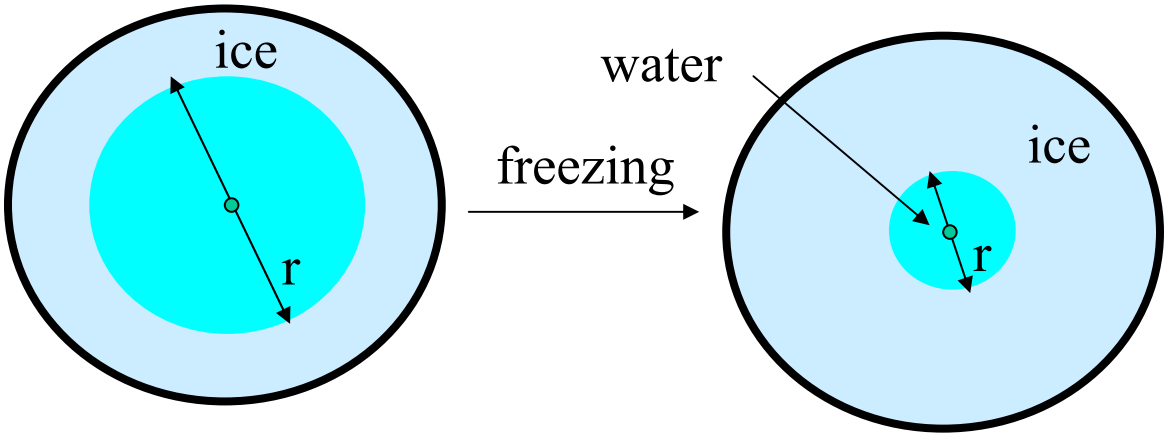

Figure 6. Decrease in effective pore cross-sectional radius upon freezing.

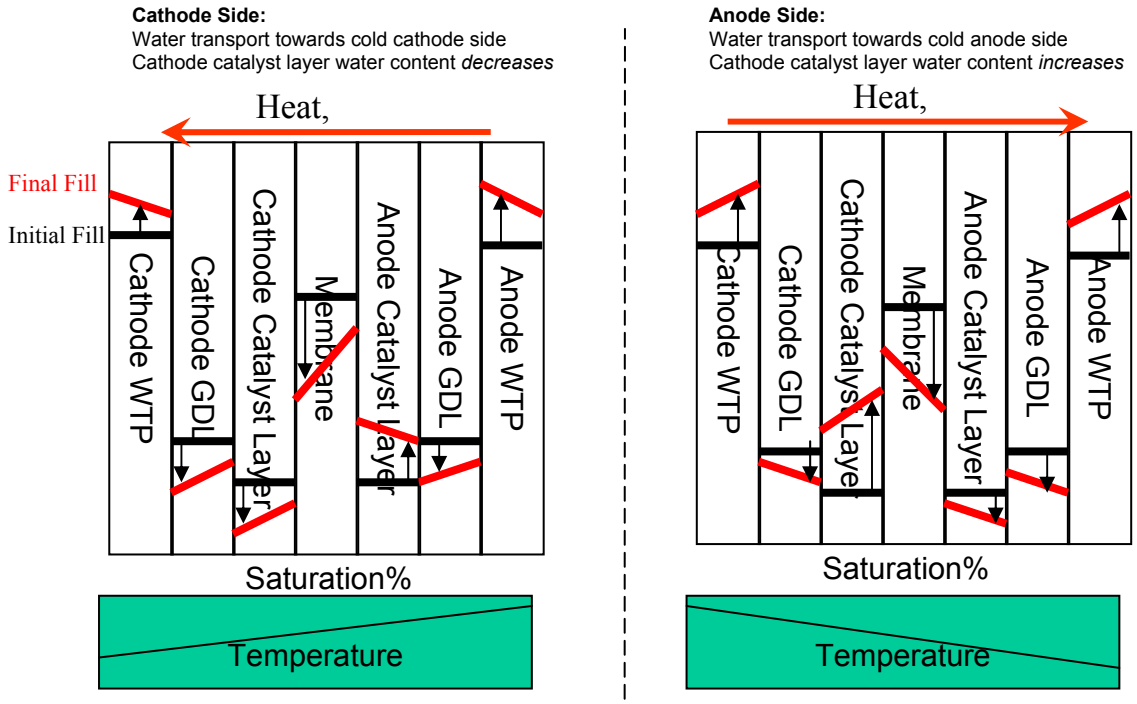

Figure 7. Schematic showing proposed effects of frost-heave mechanism at opposite ends of stack.

Single-Cell and Subscale Cold Start Test Hardware

United Technologies Research Center (UTRC) designed sub-scale and single-cell hardware (Figure 8) to simulate a cell's position in the stack during freeze and BSS. Thus, the effect of using different MEAs, GDLs, or WTPs could be evaluated before building a whole new stack. The hardware's key features were internal heating pads on each side of the cell to simulate the heat from neighboring cells, and Pyropel® insulation around the entire cell to retain most of the heat. Internal manifolds made of high-density Pyropel® were used, along with stainless steel external manifolds and pressure plates. To simulate the anode side of the stack, heat was applied to the cathode during freeze, and vice versa. The BSS can be performed with heat on both sides, or with heat on one side only, to simulate the single cell being within a stack, whereby it would be heated by adjacent cells.

Pyropel around cell

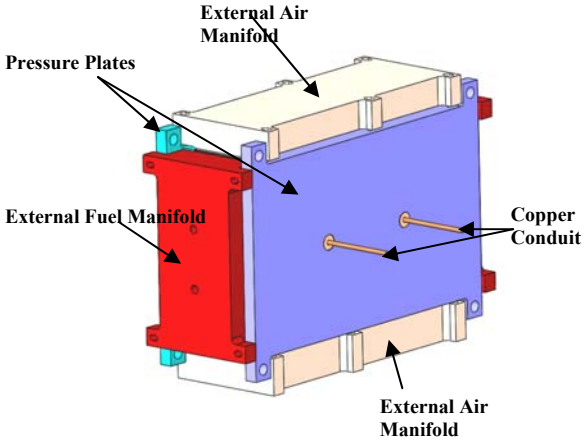

Figure 8. UTRC's insulated test hardware with internal heaters.

Effect of MEA on Cold Start Performance

The BSS performance of two different MEAs was investigated. After observing poor performance of the cells on the anode side, cells 25-30 were replaced with an alternate MEA. As shown in Figure 9, these cells showed marked improvement over the previous MEA. Interestingly, cells 19 to 24 performed worse after replacing the 5 cells on the anode end. This behavior is not yet understood, but may indicate that there is water movement, even from cell to cell.

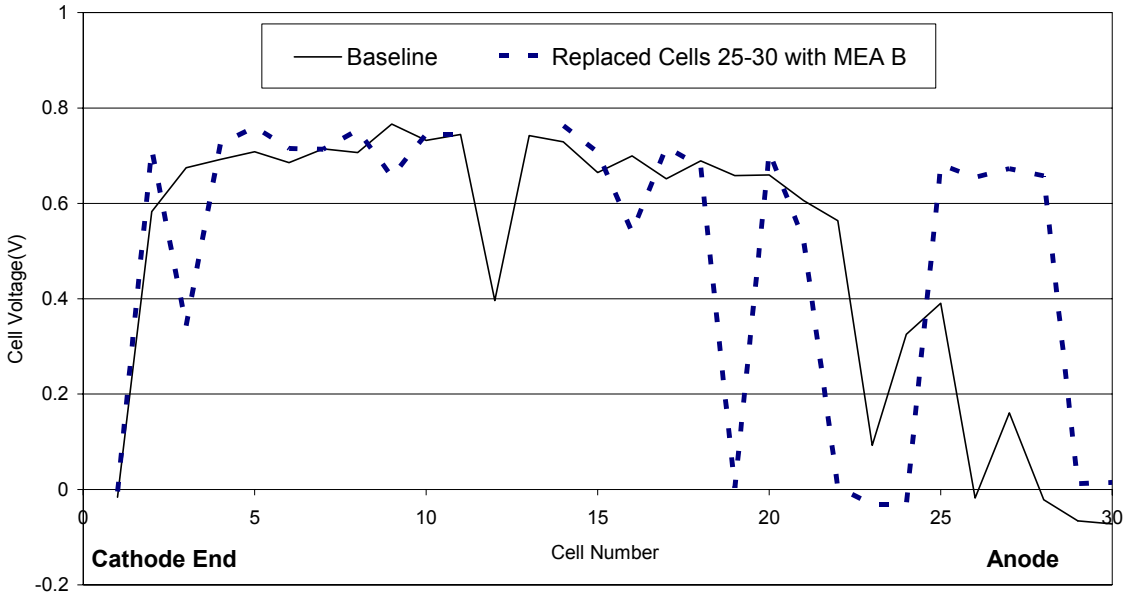

Figure 9. Short stack cell voltages 30 s after start from -10ºC (0.3 A/cm^2).

This difference in BSS performance was also observed in subscale cold start testing performed at UTRC. MEAs A (the baseline MEA) and B (alternative MEA) performed similarly after a cathode freeze (Figure 10). Both started out the BSS with positive voltage, went to approximately zero voltage (cathode hydrogen-evolution mode) within

the first minute, and stayed there for over a minute before recovering. Presumably, product water has difficulty leaving the CCL during BSS. It accumulates there, eventually blocking air access and forcing the cathode to evolve hydrogen instead of reducing oxygen. When the cell has sufficiently warmed up, water can more easily leave the CCL in the liquid and vapor state, and the cathode returns to the normal oxygen-reduction mode.

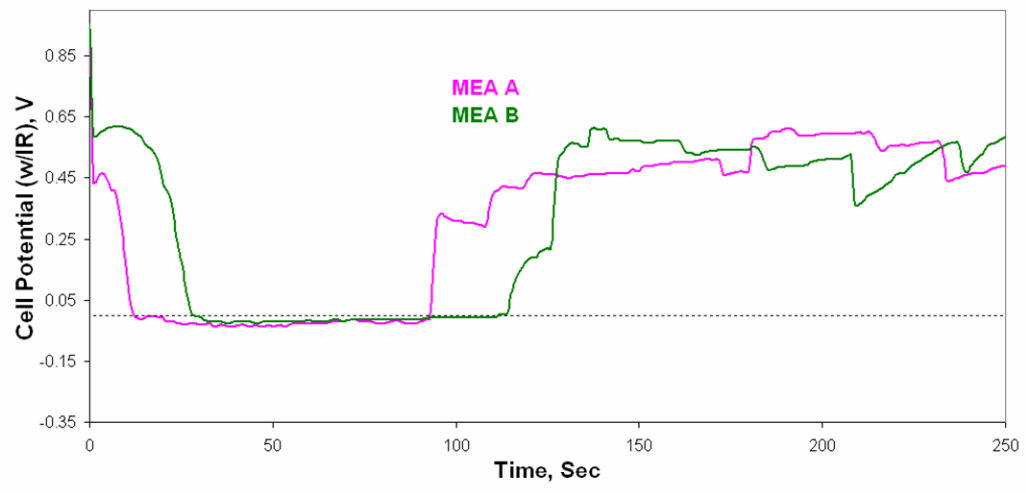

Figure 10. Sub-scale cell BSS performance after cathode freeze.

Figure 11 illustrates MEA A and B BSS performance after an anode freeze. The baseline (MEA A) cell voltage quickly drops to -0.3V, whereas MEA B stays positive for about 10 s before dropping slightly below 0 V. Both recover after two minutes of cathode hydrogen evolution. Thus, after an anode freeze, MEA B does not go to as negative a voltage as MEA A.

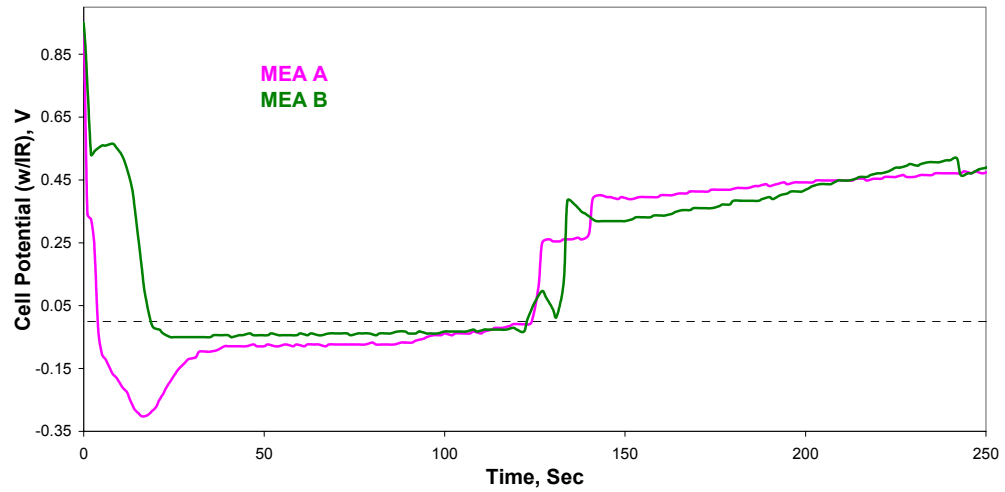

Figure 11. Sub-scale cell BSS performance after anode freeze.

The resistance of MEA A increased significantly more during an anode freeze (simulating the anode side of the stack) than during a cathode freeze (Figure 12). These results are consistent with the baseline stack results (Figure 2). MEA B cell resistance

did not increase as much as that of MEA A (Figure 13), and MEA B showed no noticeable effect of freeze direction (anode or cathode) on resistance (Figure 14).

The main difference between MEA A and B was ascertained to the catalyst layer structure, in which water accumulation is reduced for MEA B.

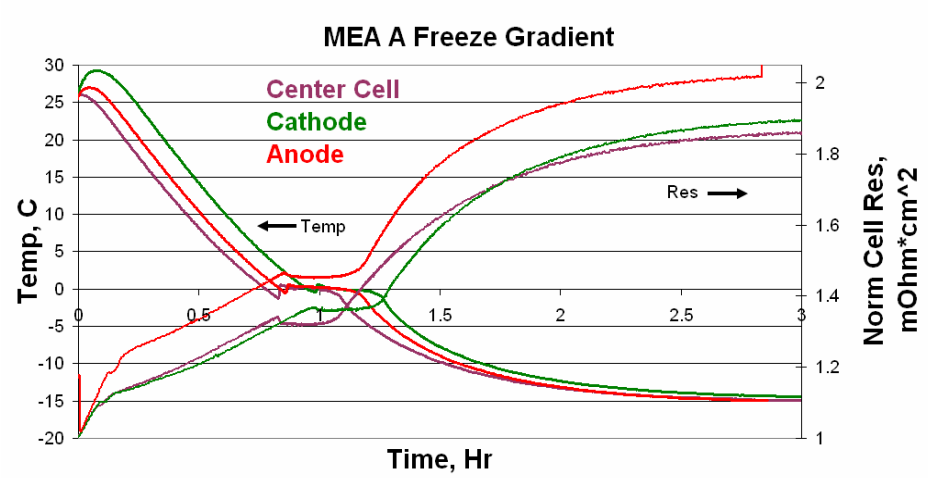

Figure 12. MEA A subscale cell resistance increase during freeze.

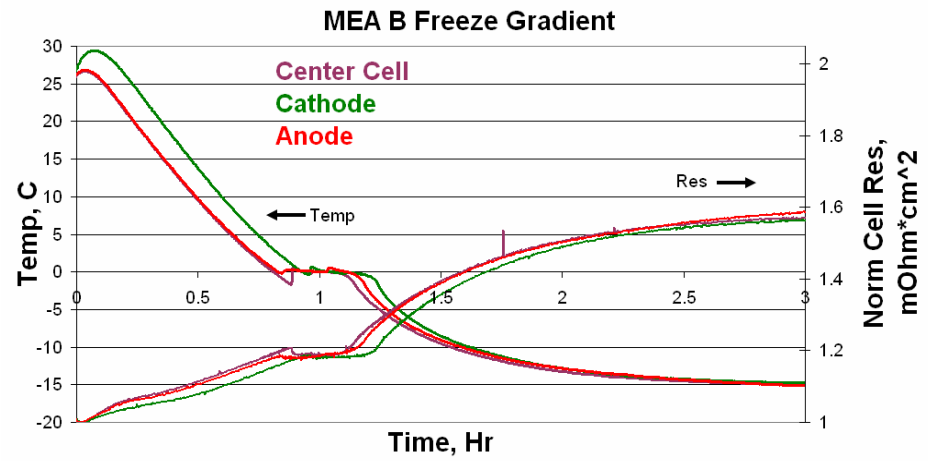

Figure 13. MEA B subscale cell resistance increase during freeze.

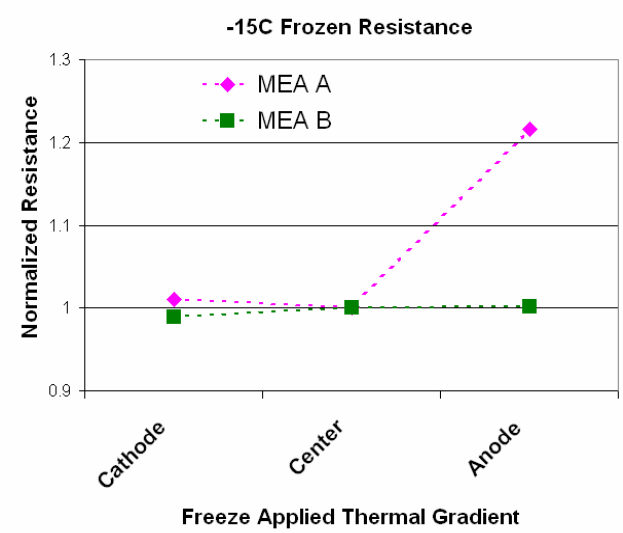

Figure 14. Effect of freeze direction on frozen resistance in sub-scale cells.

UTC Power used UTRC's single-cell hardware to characterize MEA B's performance at the single-cell level. Figure 15 shows the BSS performance of MEA B from -9 and -17ºC at 0.4 A/cm^2 after a cathode-side freeze. Figure 16 compares the BSS performance from -17ºC after an anode- and a cathode-side freeze. The BSS performance after the anode side freeze was much worse. Figure 17 shows the resistance of the cell at sub-freezing temperatures (~ -10ºC) versus the heat that was applied during the freeze. When the heat was applied to the cathode side of the cell (anode freeze), the resistance was much greater than when the heat was applied to the anode side of the cell (cathode freeze). The asymmetry in the resistance was due to an asymmetry in the physical properties of the anode and cathode GDLs. The increase in resistance is thought to have been caused by water movement that occurred during the freezing process and was exacerbated when freezing towards the anode end.

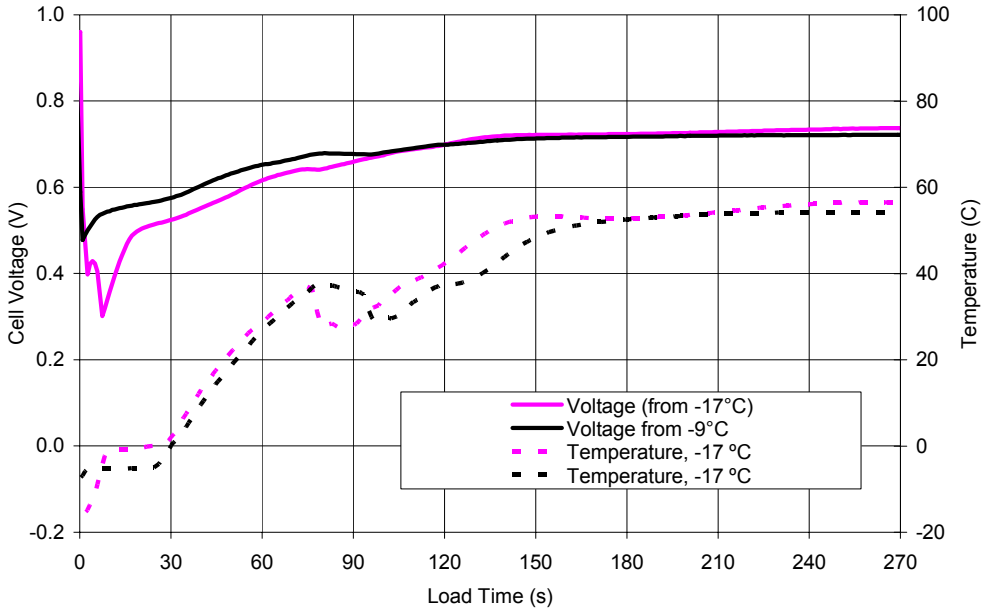

Figure 15. Effect of temperature on cold start performance of the baseline cell configuration after cathode-side freeze.

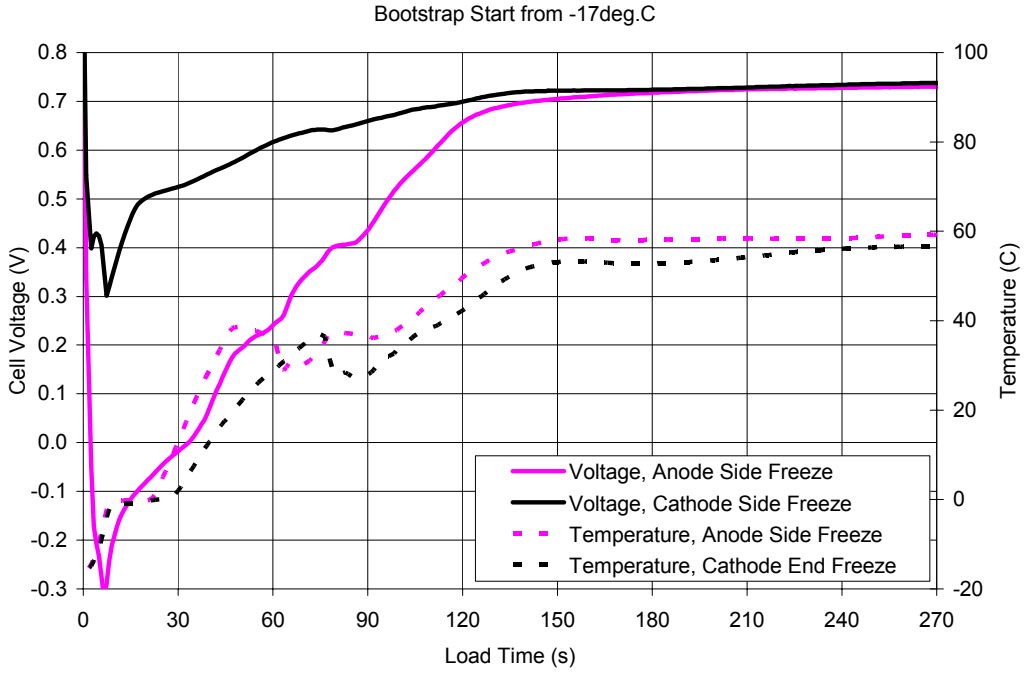

Figure 16. Comparison of anode- and cathode-side freeze on cold-start performance of baseline cell configuration.

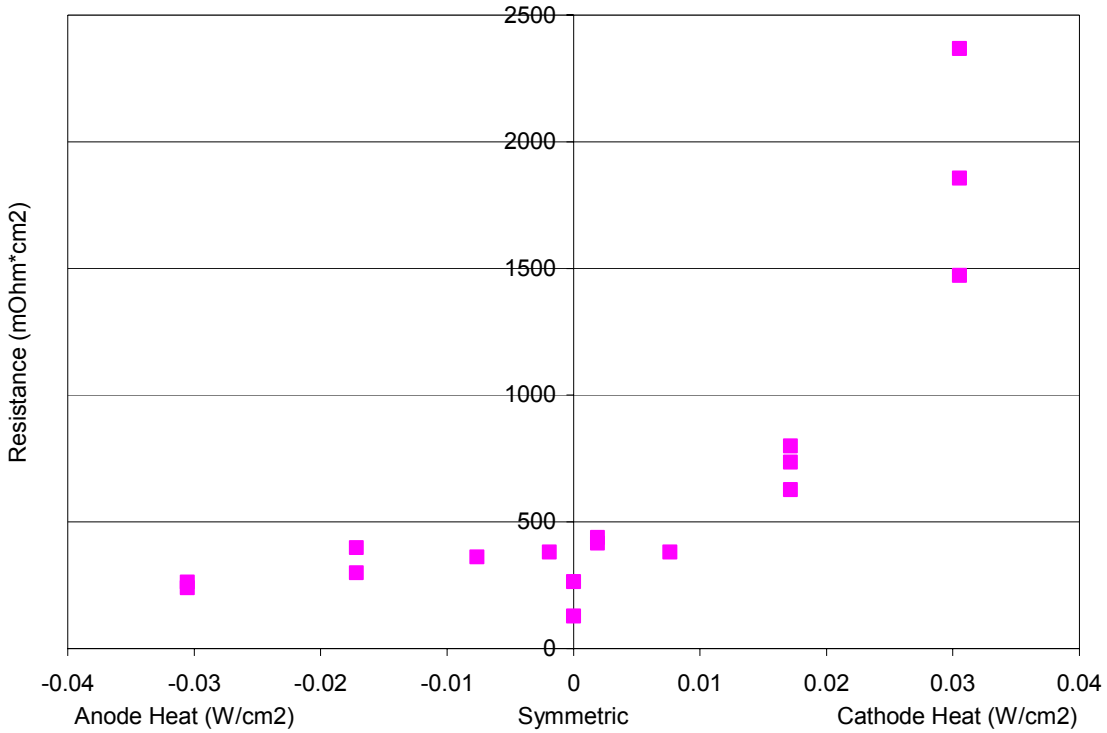

Figure 17. Effect of applied heat during freeze on cell resistance for the baseline cell configuration at -10ºC.

Effect of Gas Diffusion Layers on Cold Start Performance

To limit water movement during freeze, cells were developed with GDLs that are less permeable to water than the baseline GDL. The cells were tested at the single-cell level between pressure plates with integrated glycol coolers to induce freezing from either the cathode or anode side. To simulate the end cell effect, -10ºC glycol was fed to one pressure plate while the other pressure plate was insulated. Cells were built with low permeability GDLs on the anode and/or cathode and subject to BSS after anode- or cathode-side freeze. The cell with the low permeability GDLs on the anode and cathode performed much better than the baseline (high permeability GDLs) after an anode-side freeze, indicating that water movement from the water transport plate into the cathode catalyst layer was reduced. The worst was the cell with the high permeability anode and low permeability cathode, where the cell appeared to be ohmically limited due to drying of the membrane. For a cathode side freeze, the cell with high permeability GDLs on both sides performed the best, while the worst was the cell with a high perm anode and low perm cathode, apparently due to flooding of the cathode catalyst layer, caused by water transport from the anode side. (Figure 18).

These results corroborate the prediction that in cathode-end cells, water moves out of the CCL during freeze, while in anode-end cells, the CCL floods during freeze. By limiting water movement during freeze, low permeability GDLs inhibit both the beneficial effect on the cathode end and the detrimental effect on the anode end. Accordingly, the

baseline anode-end cells in a short stack were replaced with low permeability GDL cells. Figure 19 shows the improvement in anode-end performance that resulted from this change.

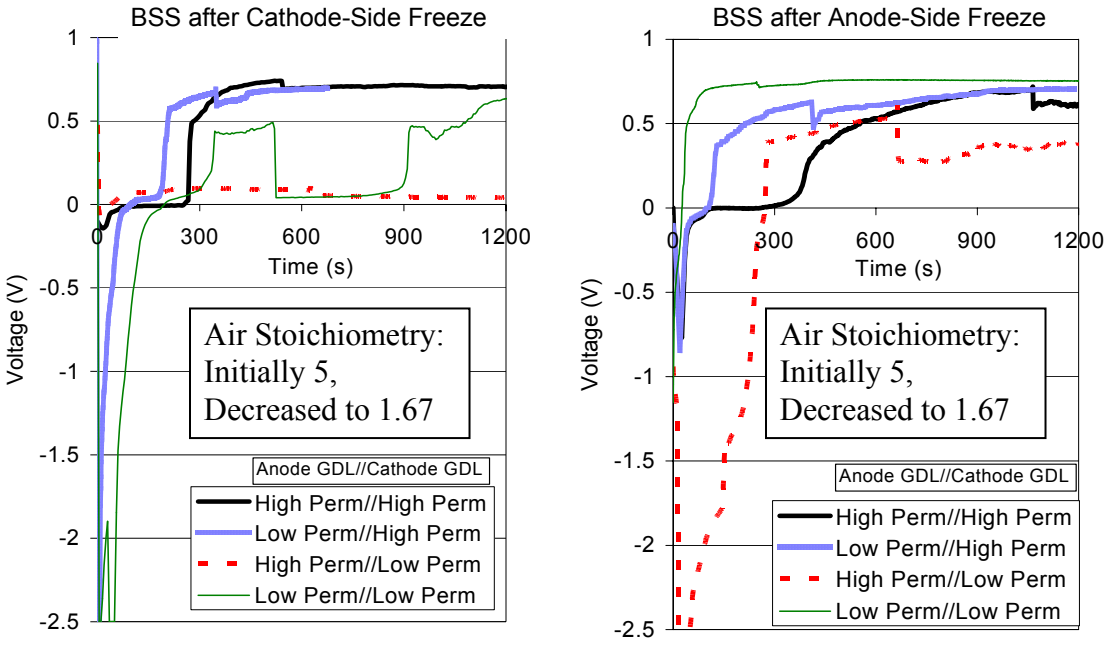

Figure 18. Comparison of frozen start performance of different cell GDL configurations after anode- and cathode-side freezes, starting up from -15°C at 0.3 A/cm^2.

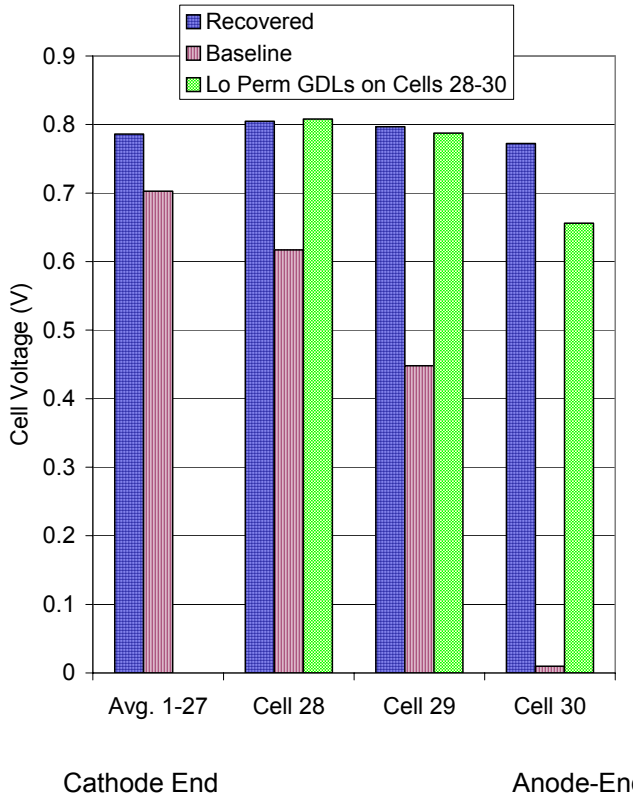

Figure 19. Comparison of cold-start performance of anode-end cells for baseline and low permeability gas diffusion layer (GDL) for short stack start from –10ºC (0.3 A/cm^2).

Next, in an effort to optimize GDL water permeability, three versions of the low permeability GDL were tested: Medium, Low, and Lowest. To obtain single-cell freezing rates similar to those observed in stacks, UTC Power tested these GDLs using the insulated test hardware. Generally, these cells were operated at a fuel stoichiometry of 1.25. The air stoichiometry was 5 during BSS and 1.67 at operating temperature. MEA B was used in each case. The following five cell configurations were built and evaluated:

Anode GDL Permeability	**Cathode GDL Permeability**
Medium	Medium
Low	Low
Lowest	Lowest
Low	Medium
Medium	Low

Some typical freeze profiles for these cells are shown in Figure 20. All the cells except the Medium Anode // Low Cathode Permeability GDL cell showed two strong freeze transitions (the flat portion of each curve and the later convex spike). Super-cooling, which is cooling of liquid-phase water below its normal freezing temperature, is thought to occur between these two transitions. The Medium // Low cell did not often show a prolonged period of super-cooling.

BSS performance is shown in Figure 21 through Figure 23. Solid lines represent BSS after anode freeze; dashed lines represent BSS after cathode freeze. The asymmetric cells exhibited the greatest impact of freeze direction. The cell with Low Anode // Medium Cathode GDL Permeability performed the best after anode freeze (solid pink), but this cell did not start after cathode freeze (not shown). The reverse configuration, Medium Anode // Low Cathode GDL Permeability, showed the opposite trend: It performed the best of all the cells after cathode freeze (dashed blue), but the worst after anode freeze (solid blue; not shown in Figure 22 due to its failure). Thus, it appears advantageous to have a Low Permeability GDL on the side from which the cell is frozen, and a medium permeability GDL on side from which the cell from which the cell is not frozen.

The symmetric cells also showed some effect of freeze direction, though not as drastic as that evidenced by the asymmetric cells. Each of the symmetric cells performed somewhat better after anode freeze (solid) than after cathode freeze (dashed). A likely explanation is that during anode freeze, water moves from the CCL to the anode catalyst layer (ACL), creating a beneficial reservoir of water on the anode side for electro-osmotic drag, and leaving empty pores in the CCL for air access, while during cathode freeze, water moves from the ACL to the CCL, drying out the ACL and flooding the CCL. The Low Permeability GDL (black) performed better than the Lowest (brown) or Medium (orange) Permeability GDL cells, suggesting that an optimum permeability exists, and that further optimization of the GDL permeability may yield further improvements in BSS performance.

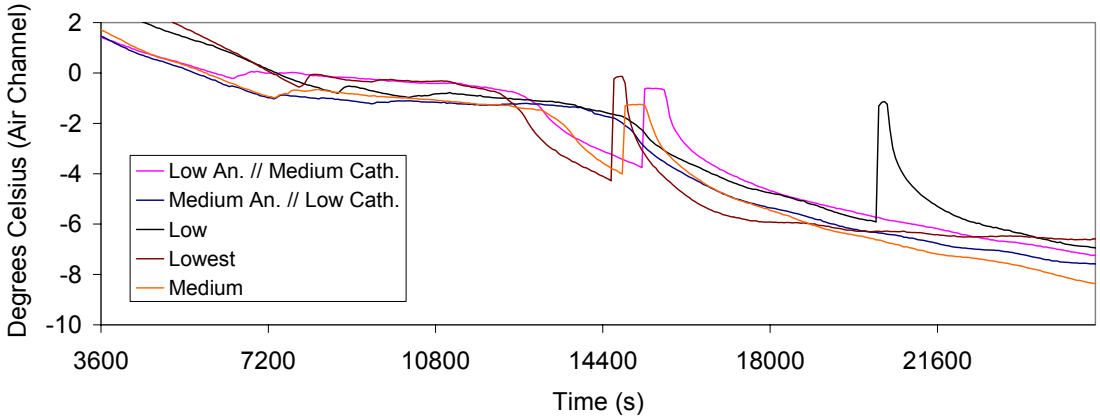

Figure 20. Temperature profile during freeze to -10°C.

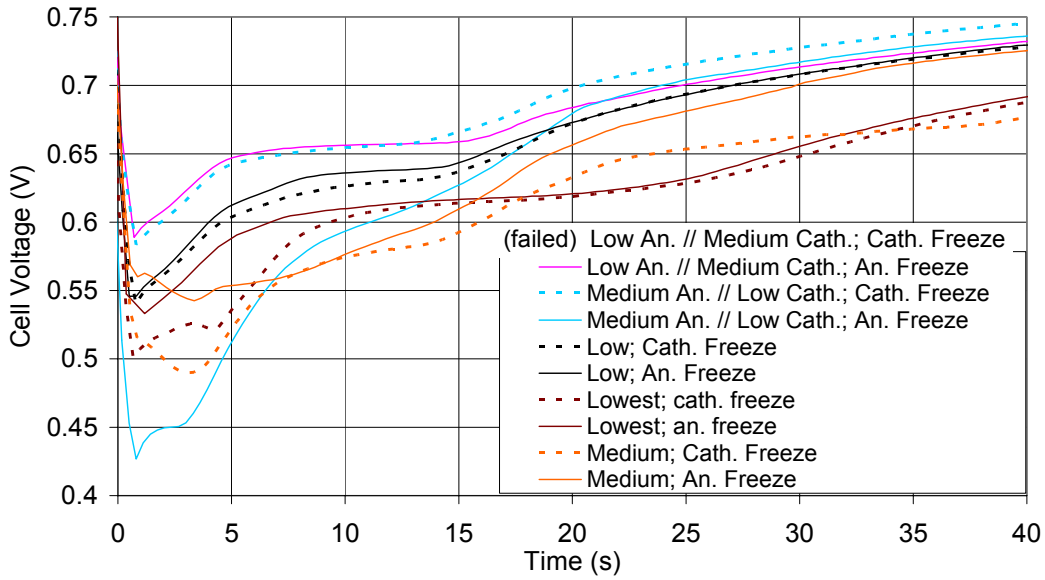

Figure 21. BSS voltage profiles during 0.6 A/cm^2 starts from -10°C.

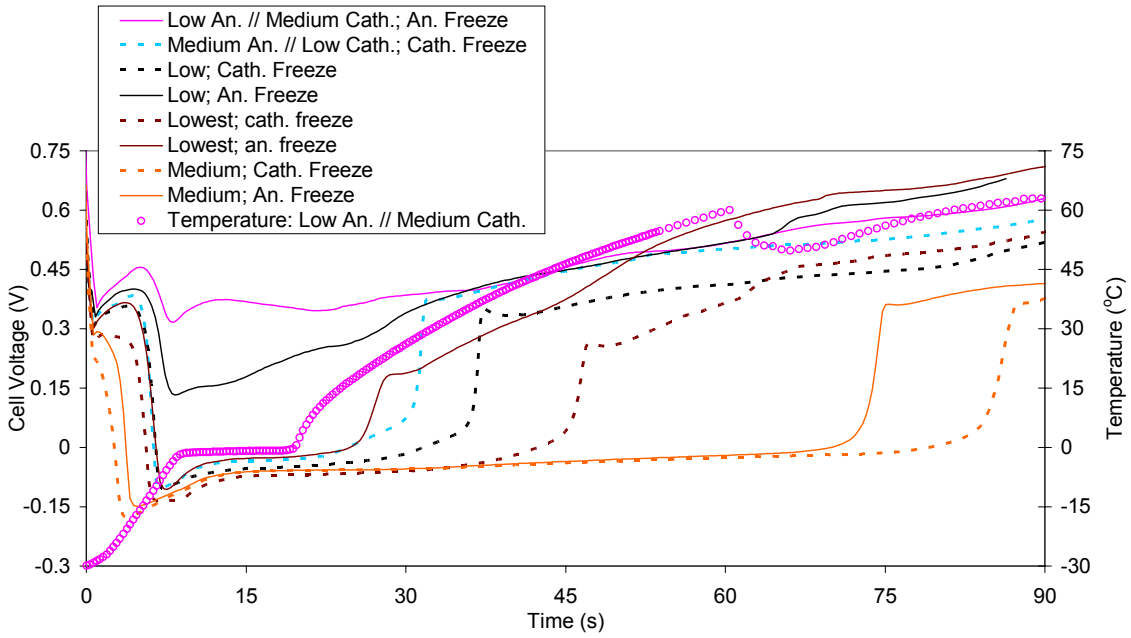

Figure 22. BSS voltage profiles during 0.6 A/cm^2 starts from -30°C.

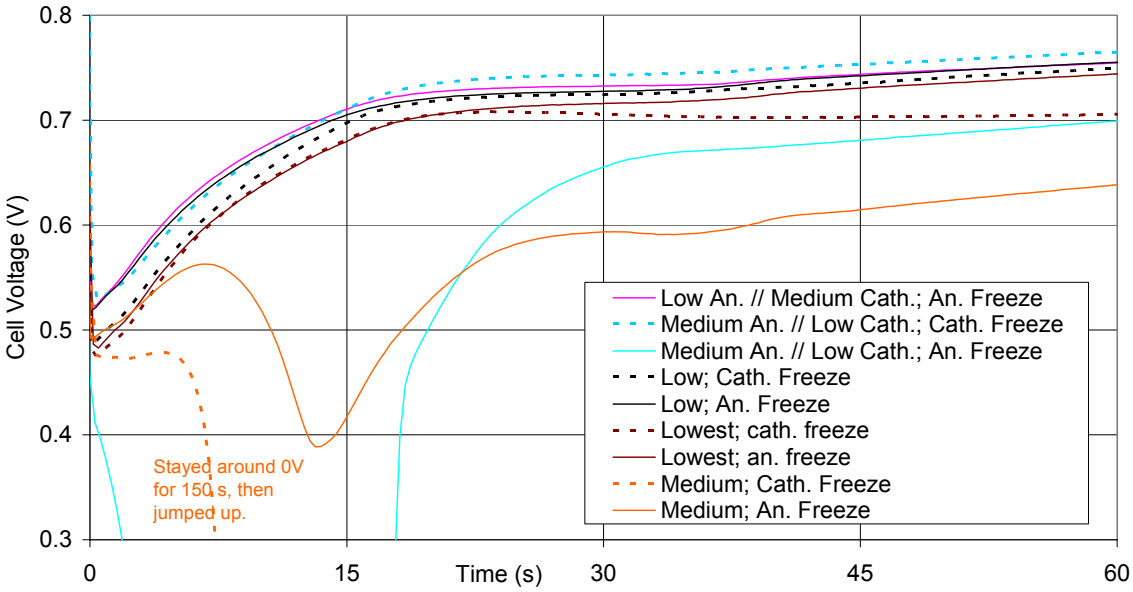

Figure 23. BSS voltage profiles during 0.3 A/cm^2 starts from -30°C.

Figure 24 and Figure 25 show that the frozen-cell resistance was highest in the cases where BSS performance was worst. To better understand this resistance increase, the resistance of the Medium Anode // Low Cathode Permeability GDL cell was monitored during anode freeze to -9°C (Figure 26). The cell resistance increased steeply as the cell super-cooled, and continued increasing steeply after the second freeze transition (at 13 h). The cell resistance continued increasing even after the cell temperature had stopped decreasing. At 21 h, the thermal gradient was reversed by switching heaters, and the resistance began decreasing even though the cell temperature remained constant at -9°C. Next, the temperature of the freezer was further decreased, and the heaters were switched again, back to anode freeze mode. The resistance increased until the cell temperature stabilized at -22°C, after which point the resistance was also stable (Figure 27). After two days at -22°C, the heaters were switched to cathode freeze mode. While the temperature was still constant at -22°C, the resistance gradually decreased over two days. The most viable explanation for this behavior is that membrane water, which remains largely unfrozen, was still moving by the frost-heave mechanism. When the cathode heater was on, water would move out of the membrane. Since the membrane water was not being replenished from the cathode side because of the low permeability of the Cathode GDL, the membrane gradually dried out, causing an increase in resistance. Then, when the temperature gradient was reversed, the water that had moved into the anode started moving back into the membrane, causing the resistance to decrease. Shorting / Crossover tests (Figure 28) and Cyclic Voltammograms (Figure 29) show lower current densities after anode freeze than after cathode freeze, possibly signifying less crossover, and therefore, a dryer membrane after anode freeze. These results suggest that partial MEA dry-out could have been a cause of BSS failure in some cases. When the cell voltage hovers just below zero for some time, the cathode is likely evolving hydrogen, indicating oxygen starvation caused by cathode flooding. If the cell starts out

at a large negative value, the cause is either due to gross fuel starvation or a large ohmic drop caused by dehydration of the membrane.

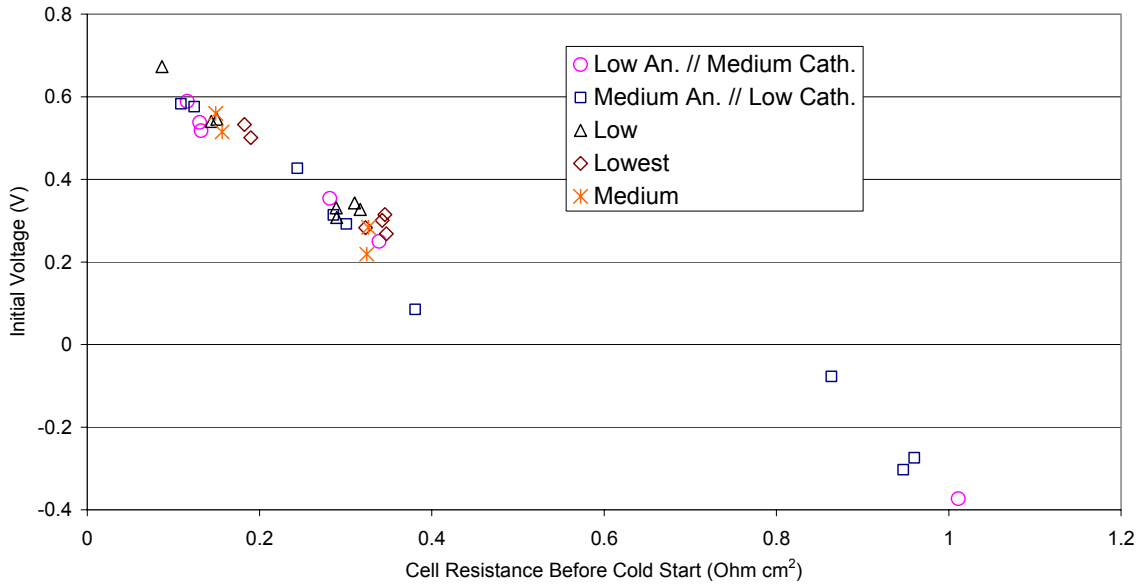

Figure 24. Voltage at beginning of 0.6 A/cm2 BSS as a function of cell resistance.

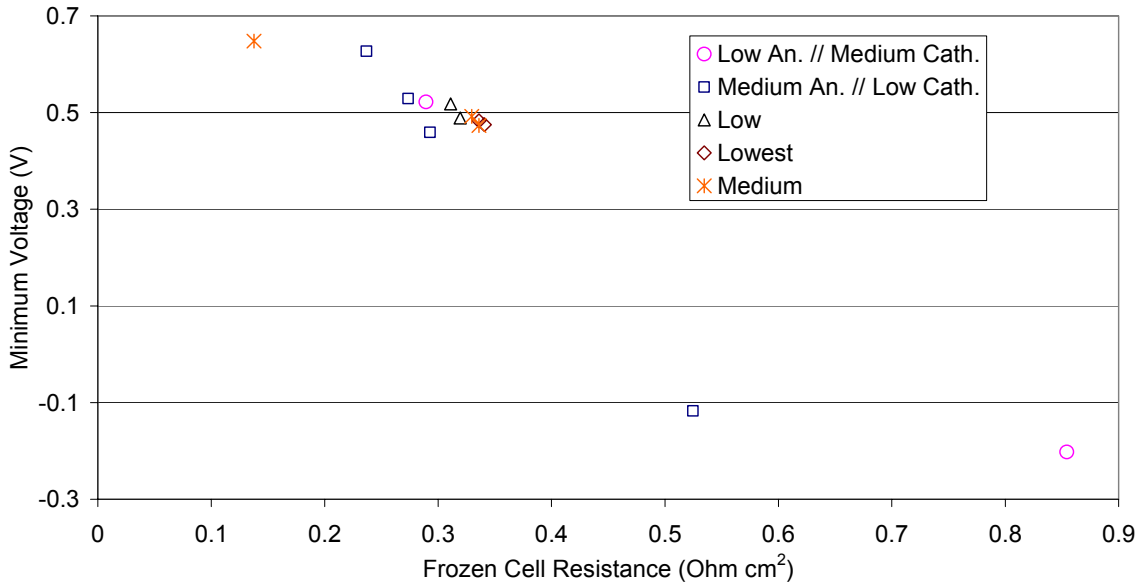

Figure 25. Minimum voltage during 0.3 A/cm^2 BSS as a function of frozen-cell resistance.

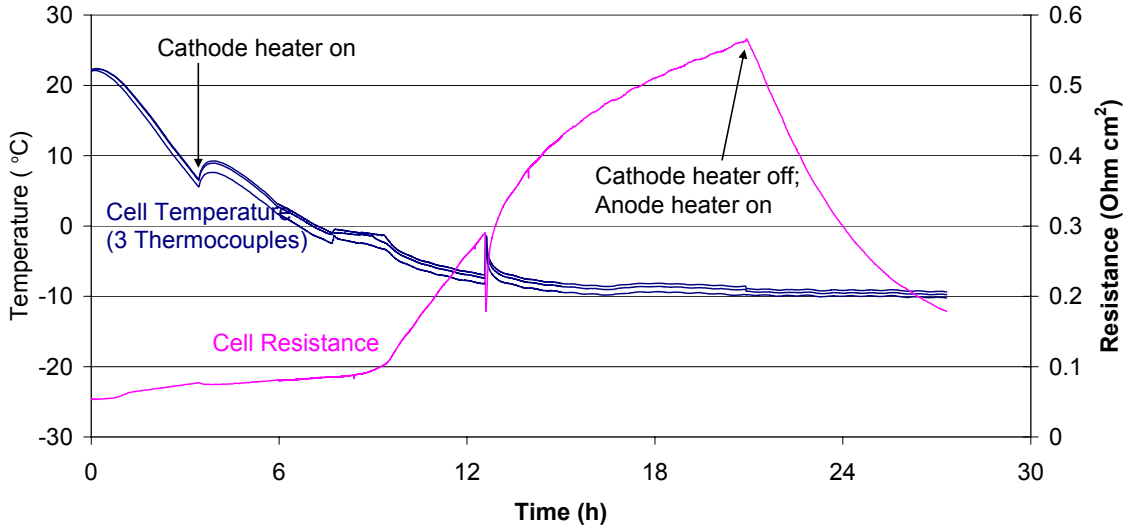

Figure 26. Resistance of Medium An. // Low Cath. Permeability GDL cell.

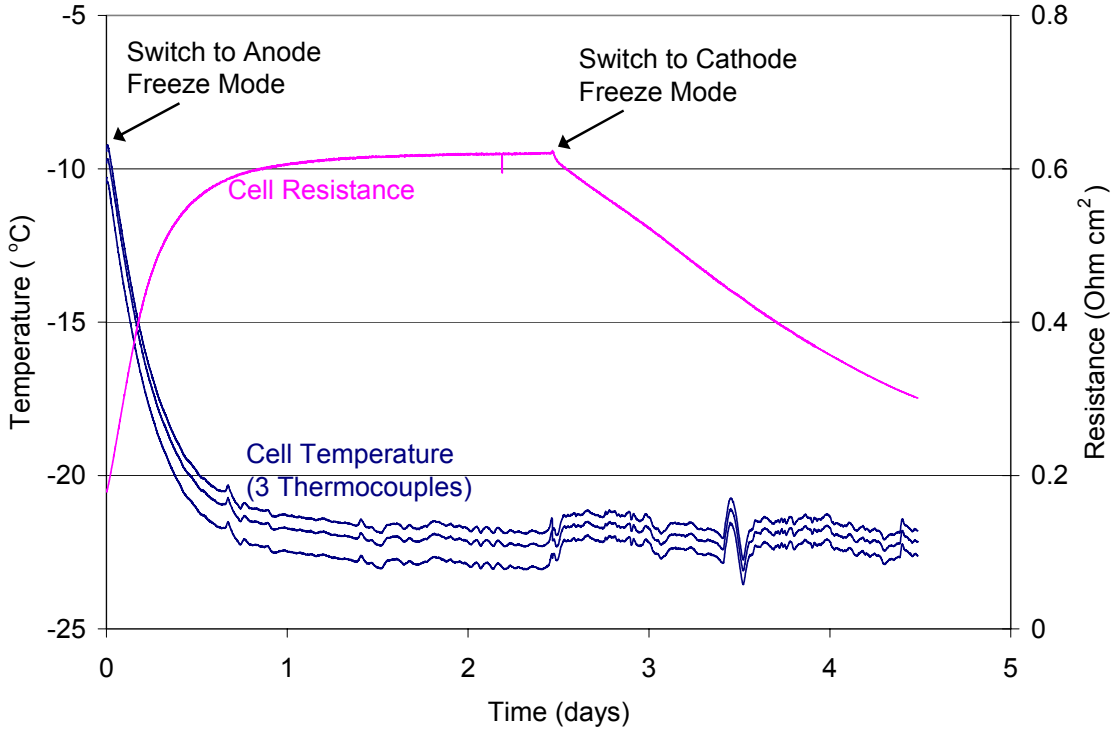

Figure 27. Resistance of Medium An. // Low Cath. Permeability GDL cell.

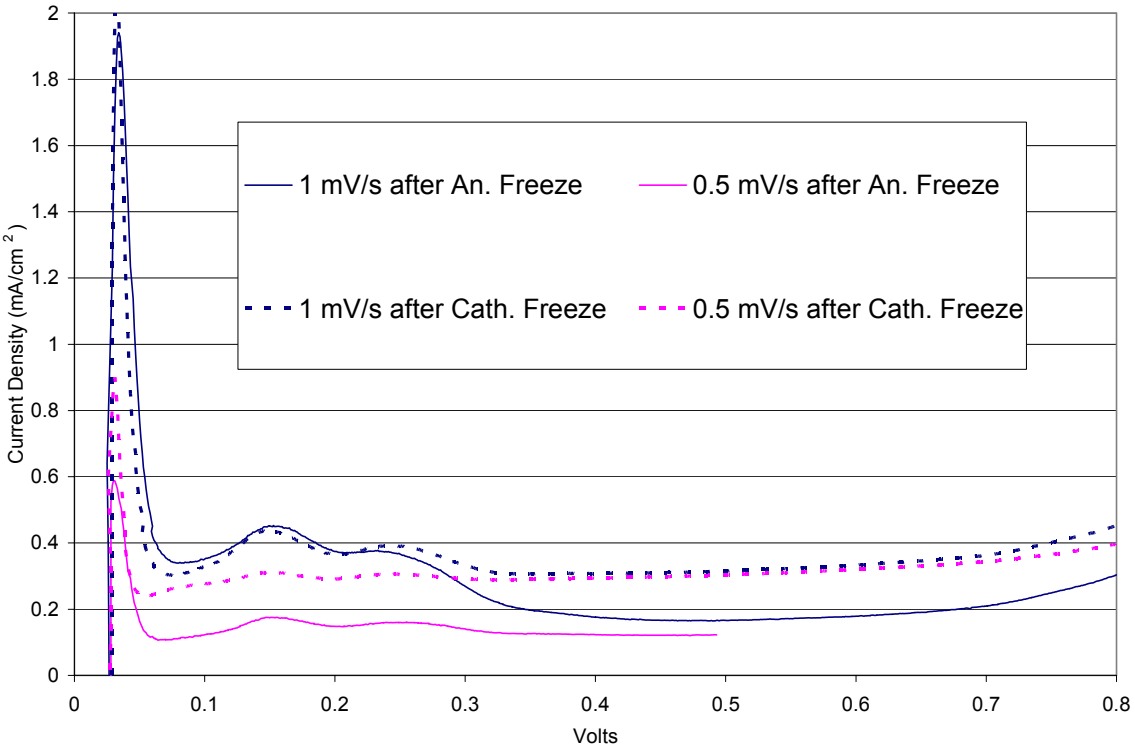

Figure 28. Shorting/Crossover at -30°C. Medium An. // Low Cath. Perm. GDL cell.

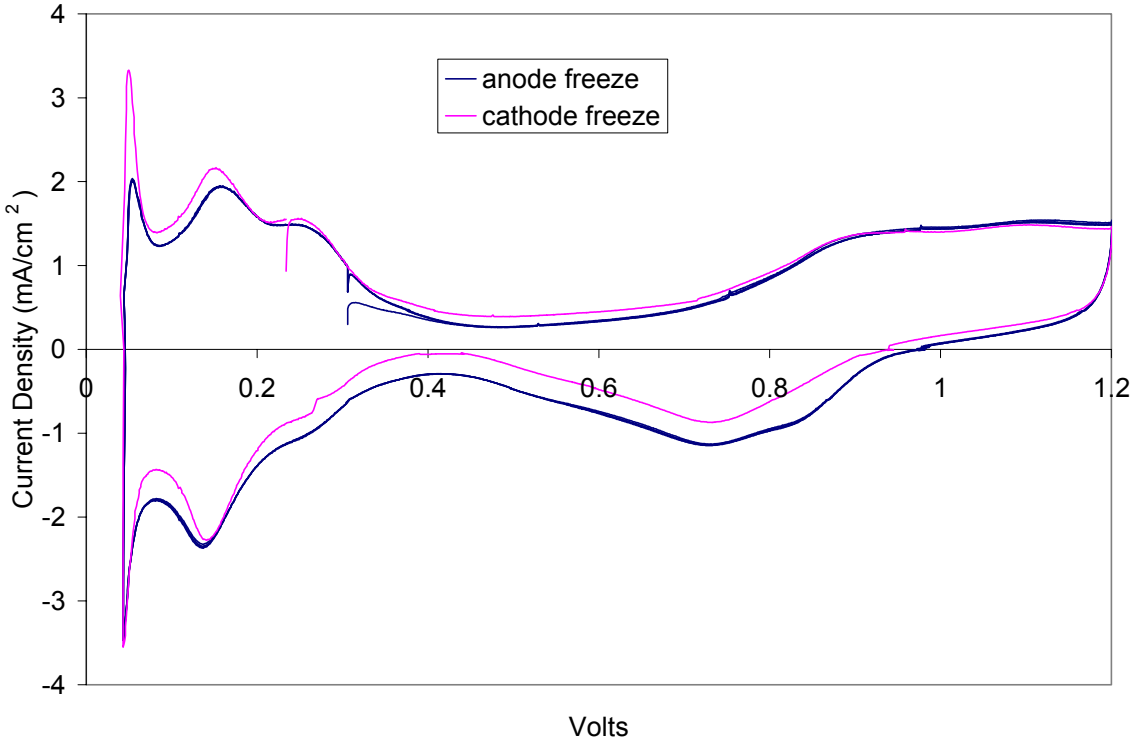

Figure 29. Cyclic Voltammogram at -30°C. Medium An. // Low Cath. Perm. GDL cell.

The normal operating temperature (65°C to 85°C) performance of each cell is shown in Figure 30. The symmetric Medium Permeability GDL cell (solid orange) performed very poorly after most BSSs and had to be hydrogen pumped to recover (dashed orange). The Low Anode // Medium Cathode Permeability GDL cell (pink) performed the best. The symmetric Low Permeability cell (black) and the Medium Anode // Low Cathode Permeability cell (blue) also performed well, especially after a cathode freeze with BSS (Figure 31). It is hypothesized that this may be due to force-filling of a few hydrophobic pores in the Low Permeability Cathode GDL which would only occur during cathode freeze. Once wet, these pores would allow for more liquid water removal from the CCL during high current density operation. However, these pores would empty again during anode freeze, accounting for the difference in performance at 1.8 A/cm^2 and 80°C after anode or cathode freeze. Hydrogen pumping negated the effect of freeze direction by emptying both the Low Permeability Cathode GDL and the CCL, thereby decreasing the t high current density performance after cathode freeze/BSS and improving the high current density performance after anode freeze/BSS (Figure 32).

In addition to BSS from frozen conditions, DOE also has an unassisted room-temperature startup requirement of 50% of rated power in 5 s. The symmetric Low Permeability GDL cell reached 613 mV in 5 s at 1 A/cm2 from room temperature, or 94% of the rated power (650 mW/cm^2). From frozen conditions, heat is usually applied to both sides of a single-cell to simulate the stack heat, but no heat was applied in this case. It should be noted that in a stack there is less thermal mass per cell than in the single cell, so this start time is expected to be conservative. The stoichiometries were 1.25 for fuel and 1.67 for air.

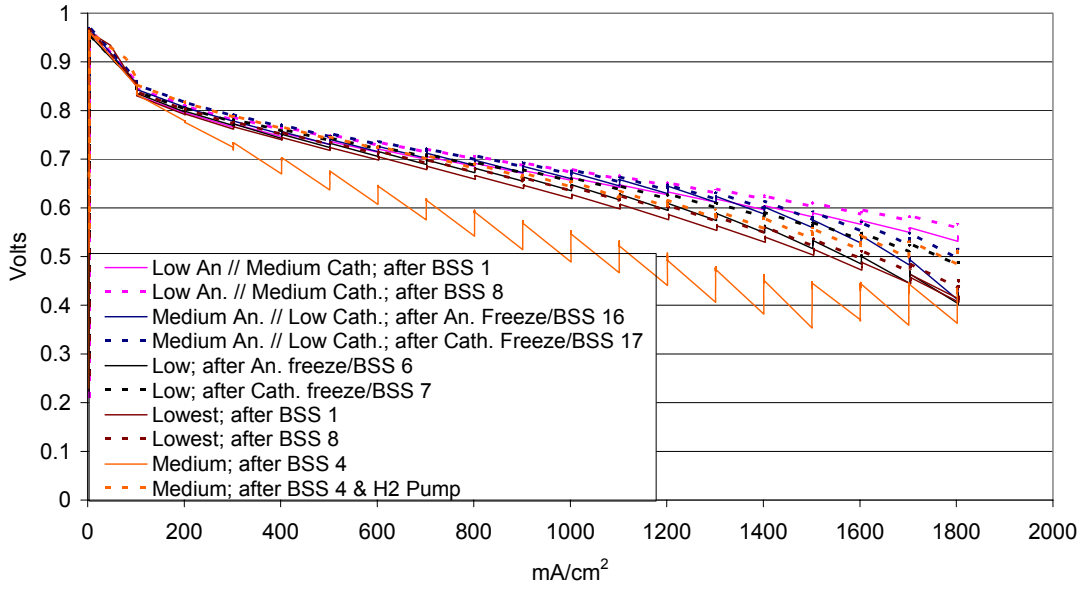

Figure 30. Normal operating temperature performance of various GDLs.

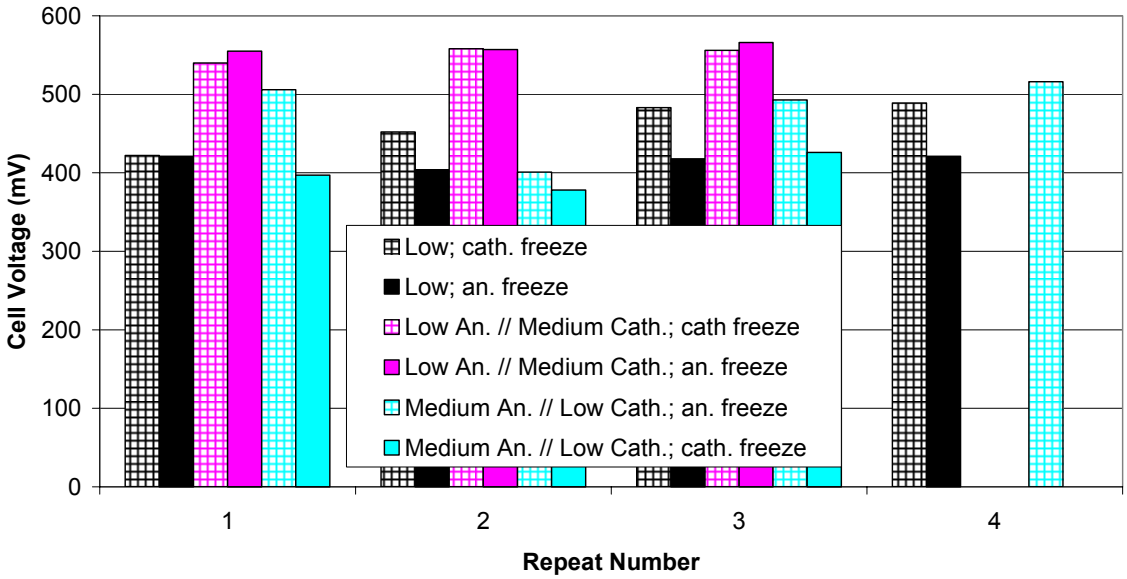

Figure 31. Performance at 1.8 A/cm^2 and 80°C vs. Freeze Direction.

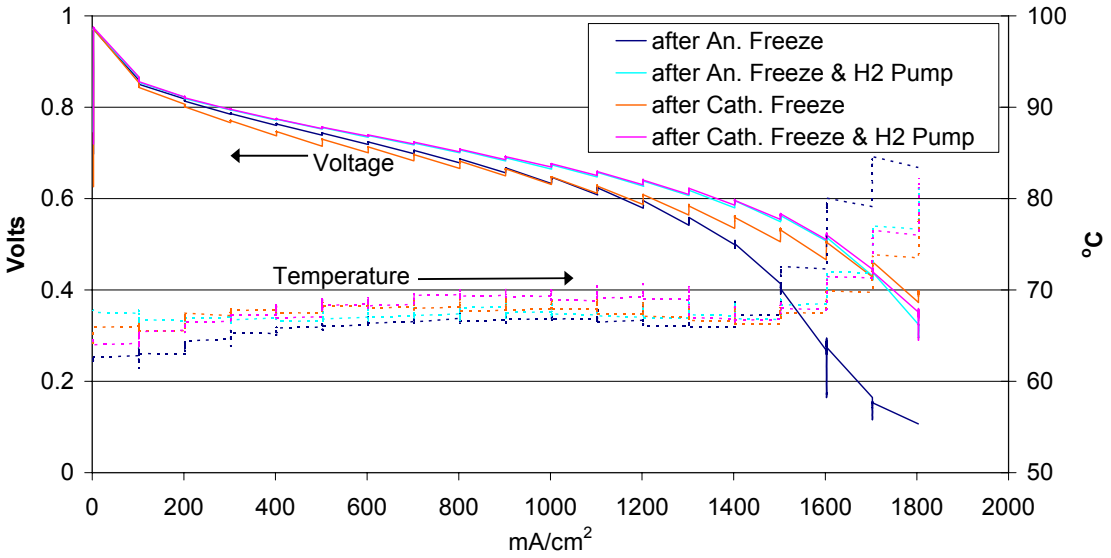

Figure 32. Medium An. // Low Cath. Permeability GDL cell.

Effect of Cell Thermal Mass on Cold Start Performance

The effect of reducing the mass of the cell was investigated by lowering the water content in the bipolar plates. The reduced thermal mass was expected to enable a more rapid increase in the cell temperature from a frozen condition, improving the start-time performance. The first variant, Variant A, used the low thermal mass configuration along with MEA B, but kept the baseline high permeability GDLs. Variant A had better cold-start performance than the baseline cell / MEA B configuration after an anode freeze (Figure 33). Since the temperature rise was approximately the same as the baseline, the difference in the cold start performance was actually due to the difference in water

management rather than thermal mass. The performance after a cathode-side freeze was the same as the baseline cell configuration (Figure 34). Figure 35 compares the BSS performance of Variant A versus freeze direction. Unlike the baseline cell configuration, there was little effect of the freeze direction for this cell configuration. This was due to the lower water content of this cell configuration. There was also no effect of freeze direction on cell resistance changes during the freeze process, unlike the baseline cell configuration, which also suggests less water movement in Variant A (Figure 36). Variant A performed well during a 0.8 A/cm^2 BSS after cathode- and anode-end cell freezes (Figure 37). An attempt was made to start from -30°C, but the cell failed to start, although no permanent damage was seen after the cell was thawed.

After separately investigating the possible benefits of low permeability GDLs and of low thermal mass cell configurations, a single-cell (Variant B) was built with both of these features. Figure 38 shows the BSS performance at 0.6 A/cm^2 from -30ºC of variant B after an anode-side freeze. The cell reached 50% rated power (at a useful voltage) at approximately 40 s, which was significantly better than variant A, which could not start from -30ºC. Figure 39 shows the BSS performance from -30ºC after a cathode-side freeze. The performance was much worse than after the anode-side freeze. It did not reach 50% rated power at a useful voltage until after approximately 100 s. In this test, the current density was gradually increased in order to produce the maximum heat. The changing current and temperature, as well as the thawing ice, resulted in the observed voltage fluctuations.

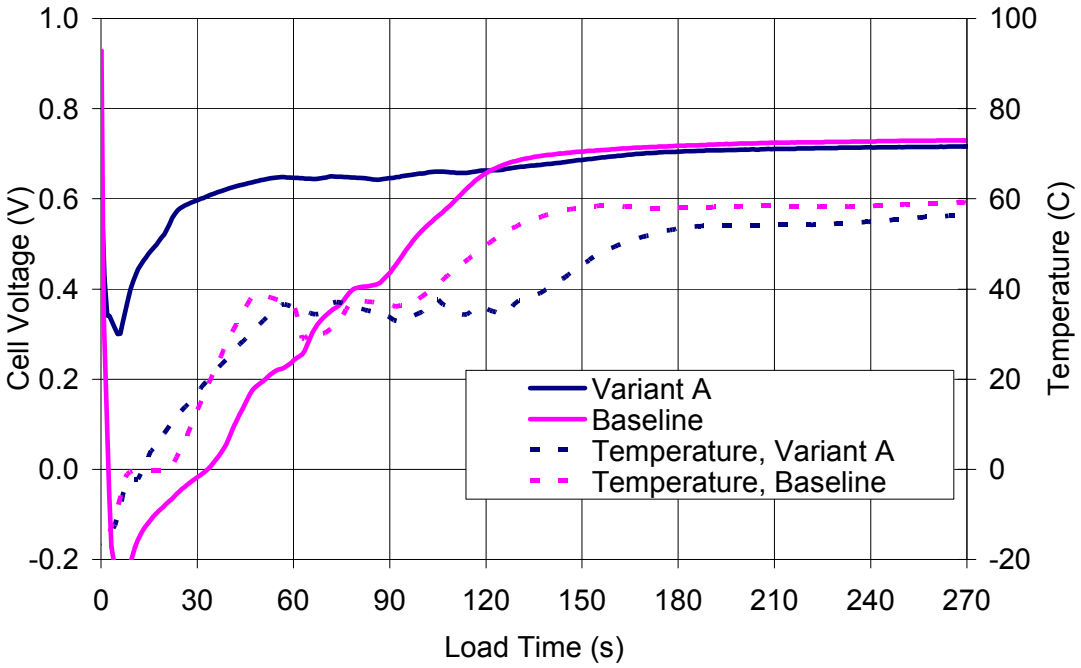

Figure 33. Comparison of cold-start performance of variant A to baseline cell configuration after anode-end cell freeze (400 mA/cm^2, -17 ºC).

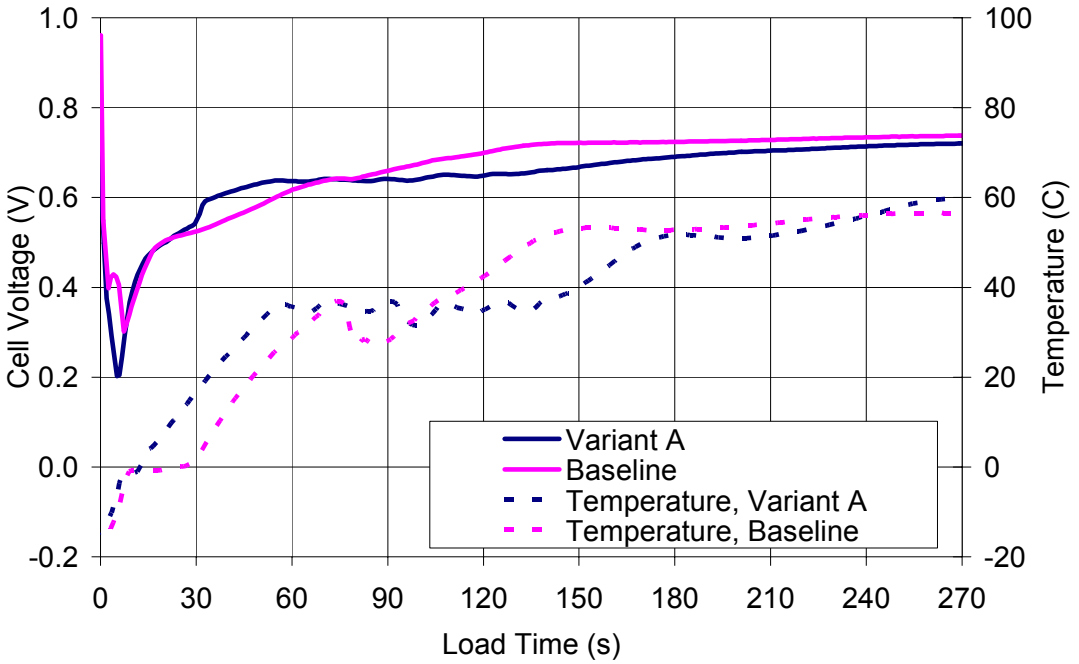

Figure 34. Comparison of cold-start performance of variant A to baseline cell configuration after cathode-end freeze (400 mA/cm^2, -17 ºC).

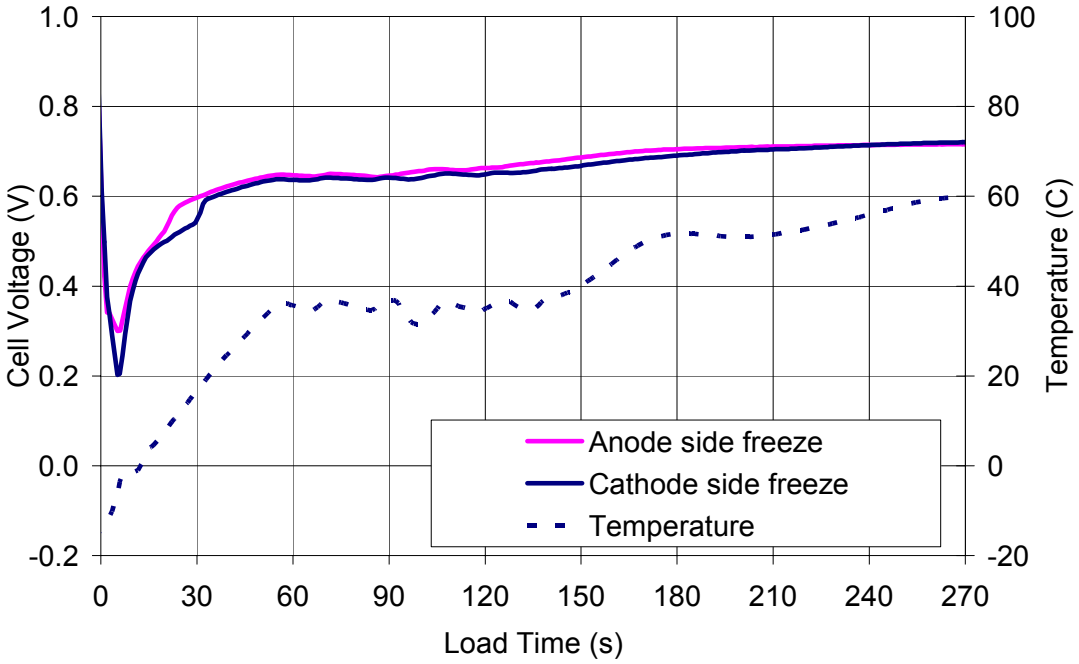

Figure 35. Effect of freeze direction on cold start performance for variant A (400 mA/cm^2, -17 ºC).

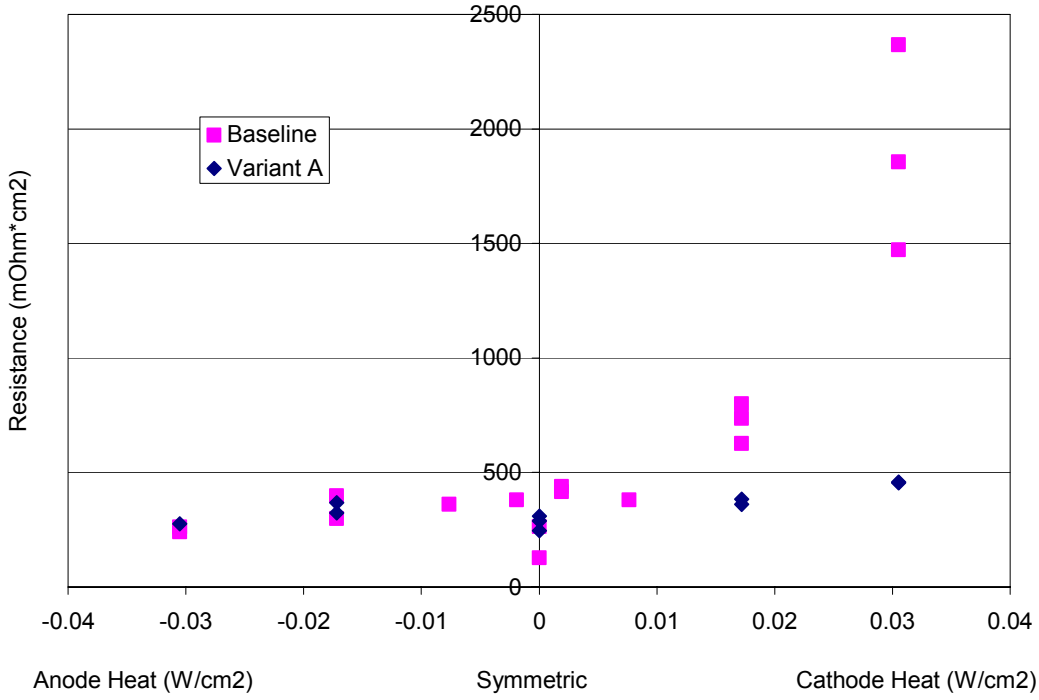

Figure 36. Comparison of the effect of applied heat during freeze on resistance changes for Variant A and the baseline cell configuration.

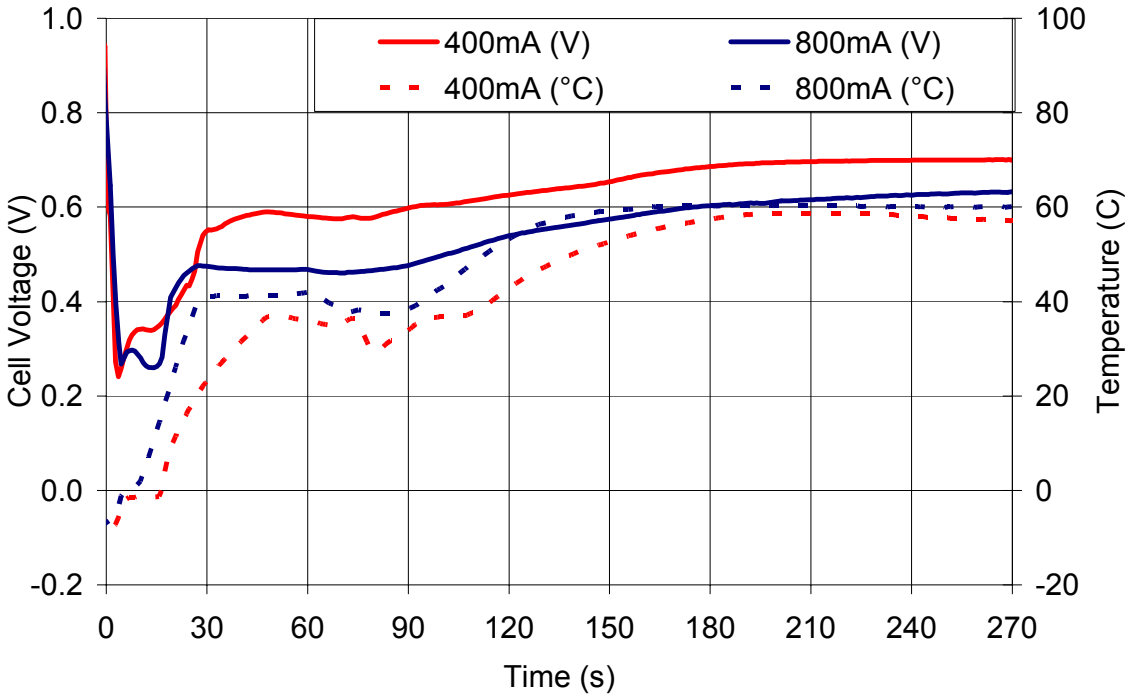

Figure 37. Effect of current density on cold start performance for variant A (-10 ºC).

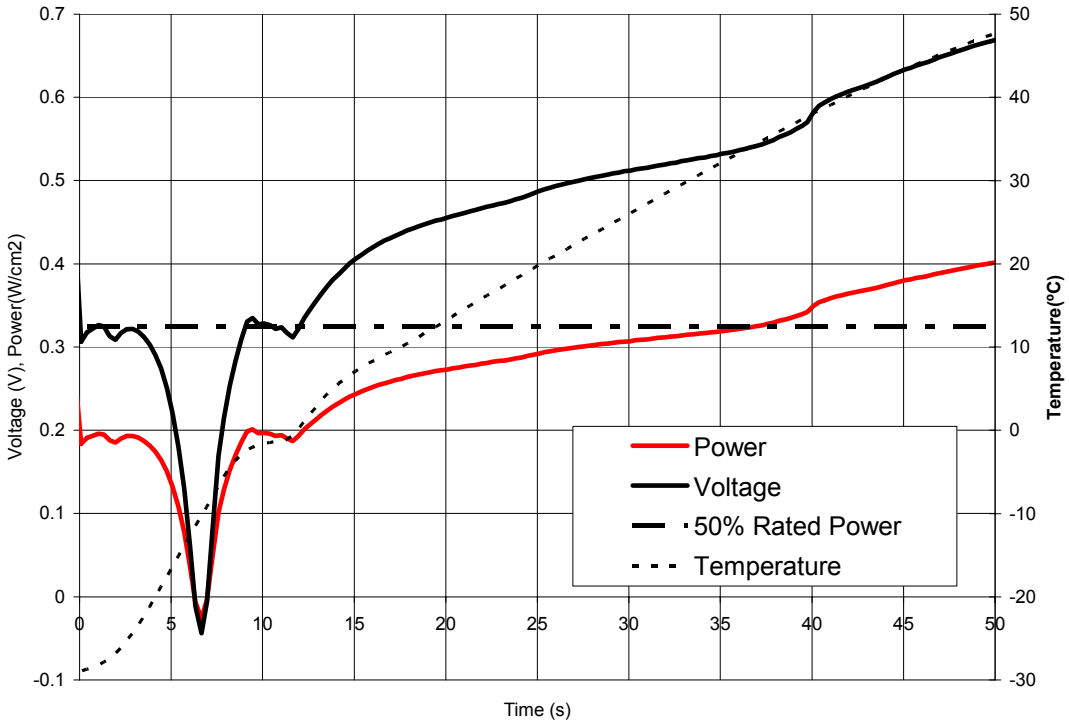

Figure 38. Cold start performance of variant B at 600 mA/cm^2 from -30 ºC after anode side freeze.

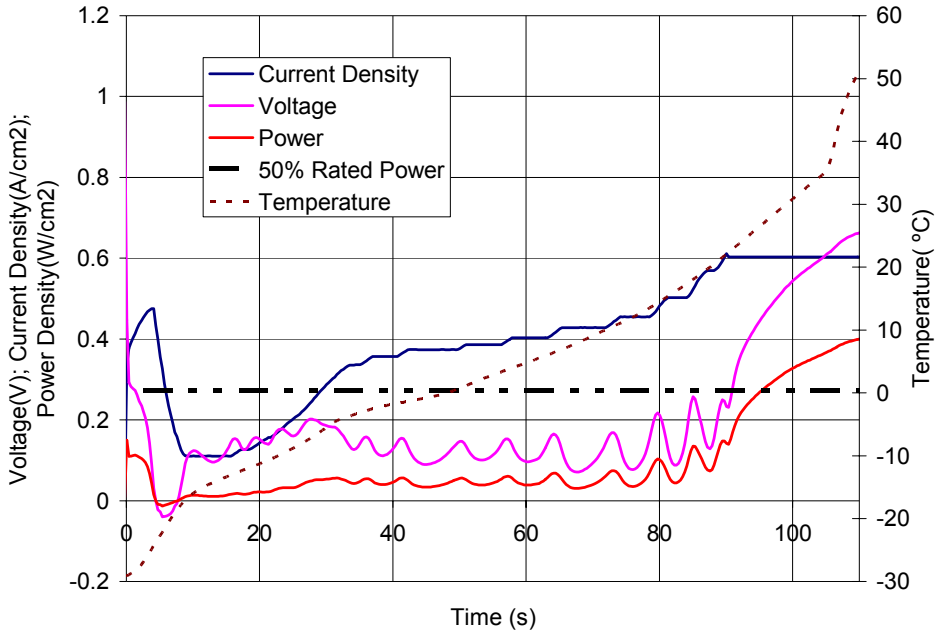

Figure 39. Cold start performance of variant B from -30 ºC after cathode freeze.

Variant B, which had both low permeability GDLs and low thermal mass cell configuration, did not perform as well as cells with low permeability GDLs and baseline cell configuration. For example, the low permeability GDLs with baseline cell configuration were consistently start at 0.6 A/cm^2 from -30°C after an anode-side freeze. The low thermal mass configuration could not perform consistently at 0.6 A/cm^2 from -30°C. Thus, it appears that simply using low permeability GDLs with baseline cell configuration is a better option than using the low thermal mass configuration with either low or high permeability GDLs.

Cold Start Durability and Freeze-Thaw Survivability

A single-cell with the low permeability GDL, MEA B, and baseline cell configuration was subjected to 17 cold starts. As shown in Figure 40, no loss in performance was observed. A short stack was also subjected to over 20 cold starts. Figure 41 shows the performance at 1 A/cm^2 after repeated cold starts. No loss of performance was observed after 25 cycles.

A 20-cell stack was subjected to more than 100 freeze-thaw cycles to -40ºC. A typical freeze-thaw profile is shown in Figure 42. Figure 43 shows that stack performance was unaffected by freeze-thaw cycling. On the end-cells, some recoverable decay was observed. Figure 44 shows SEM micrographs taken after freeze/thaw cycling. No structural damage was observed in either the membrane or catalyst layers.

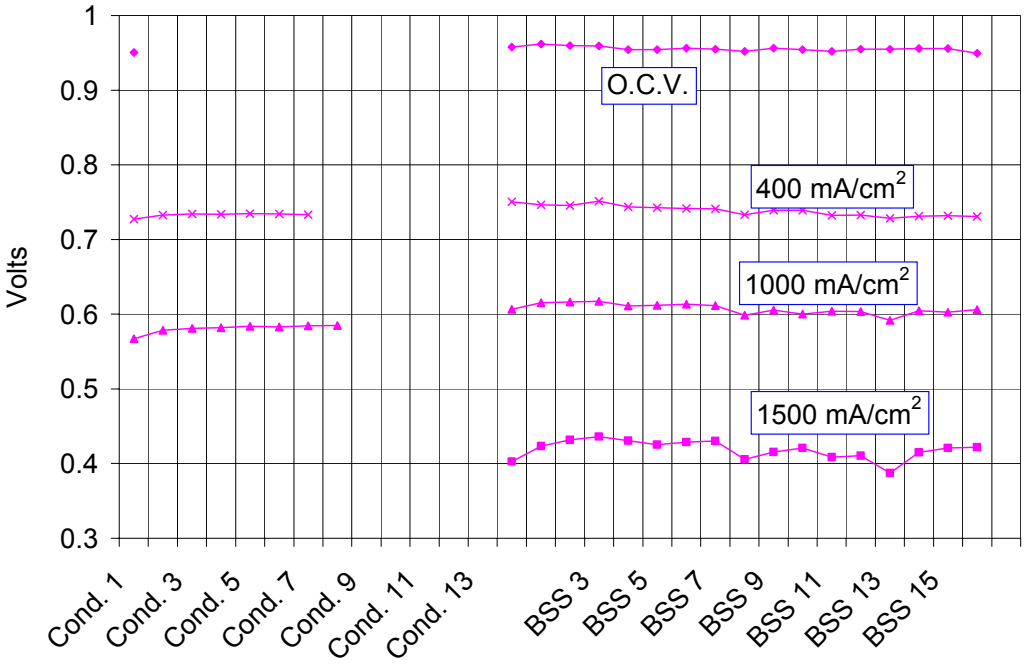

Figure 40. Performance of baseline cell configuration after repeated cold starts.

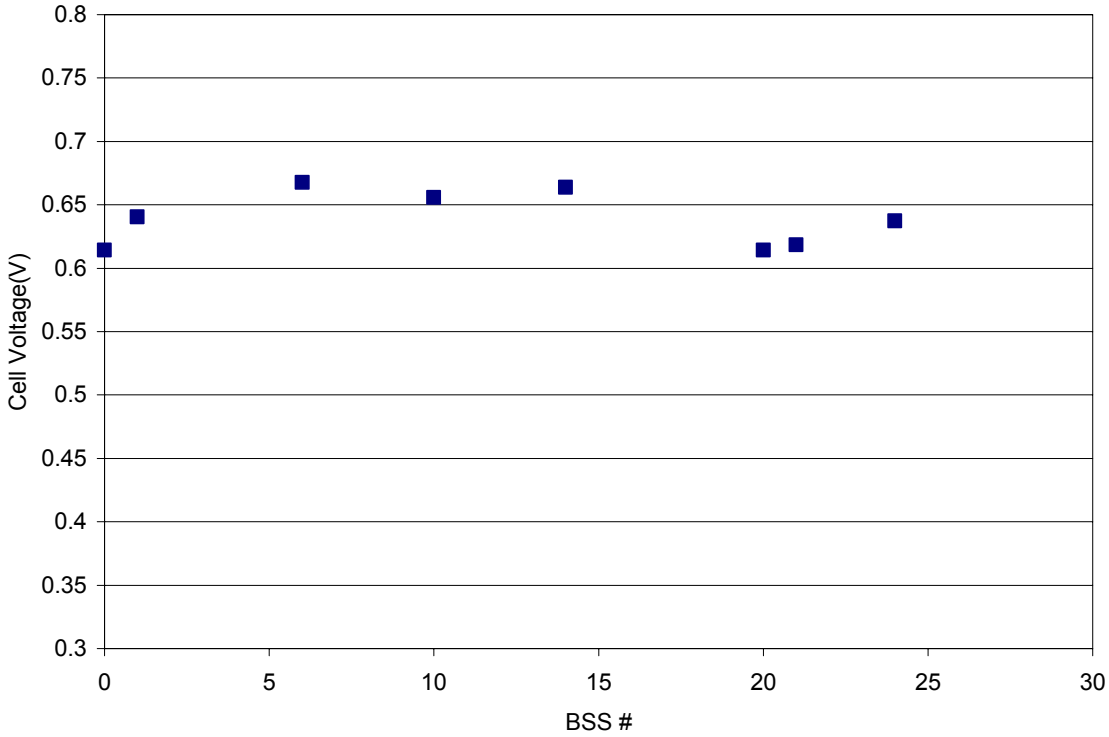

Figure 41. Performance of a short stack after repeated cold starts (1 A/cm^2, 1.2//1.66 Stoich.).

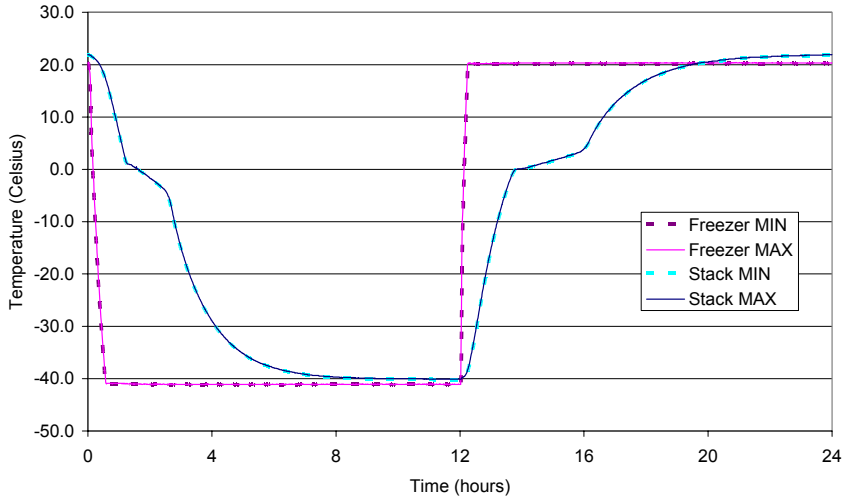

Figure 42. Temperature profiles of freezer and stack during freeze-thaw cycling.

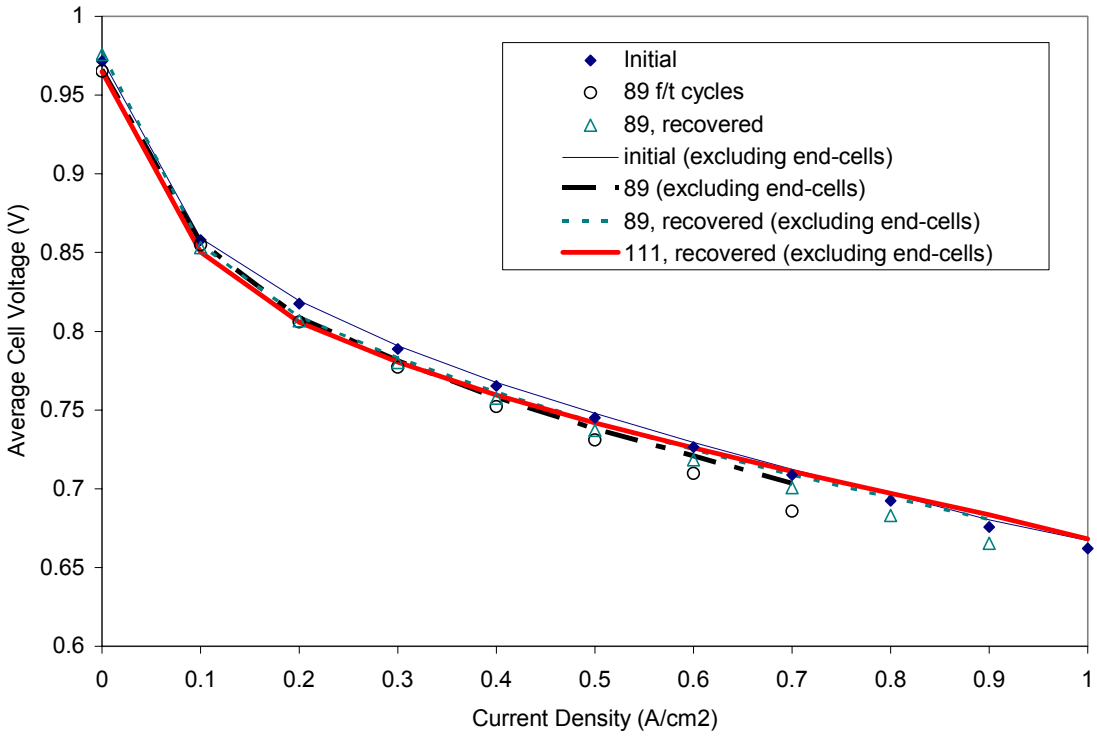

Figure 43. Performance and freeze-thaw cycling of second short stack.

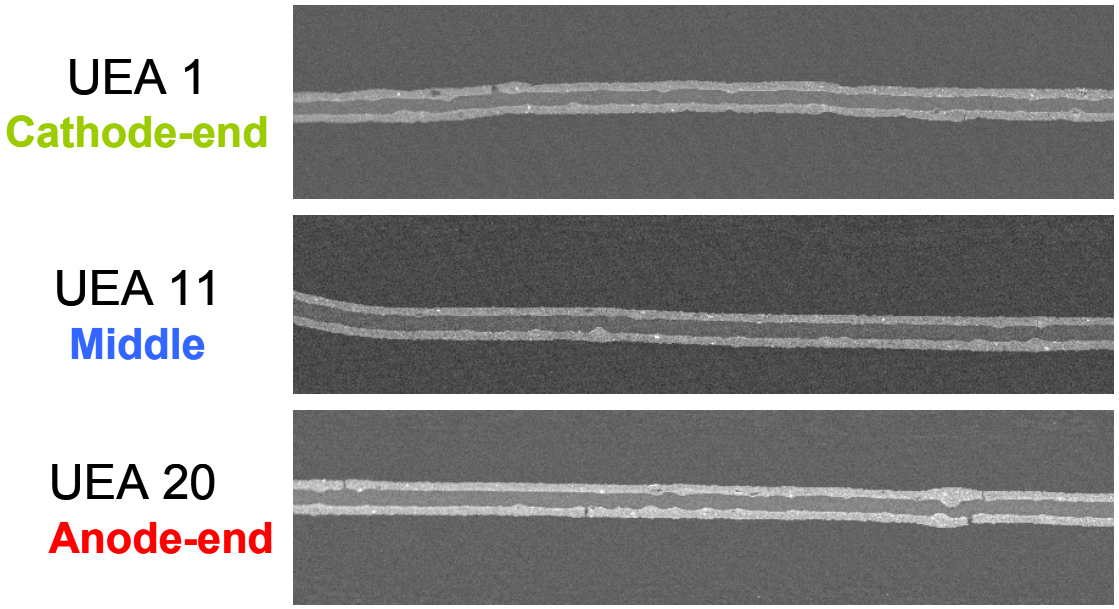

Figure 44. Scanning Electron Micrographs (SEM) of short-stack after 100 freeze-thaw cycles.

Progress *vs.* 2010 DOE Targets

UTC is committed to achieving and surpassing key low temperature targets set by DOE and the major automotive OEMs. DOE targets and UTC internal targets, along with the current UTC capability, are listed in the table below. We have reached 47% rated power in 30 sec after an anode side freeze. The start performance after a cathode freeze is slower, only reaching 34% rated power after 30 seconds. The difference has been attributed to water movement during the freezing process.

UTC has already exceeded the survivability target at the short-stack level, completing over 100 freeze-thaw cycles to -40°C with negligible performance loss in all cells but the very end cells.

DOE also has a target of 50% rated power in 5 s from normal room temperature. UTC has achieved 94% rated power in 5 s from room temperature, with no simulated stack heating and with standard utilizations in a single-cell apparatus.

The results presented here suggest that further optimization can be performed on GDL permeability, start procedures, stack and system design, and other aspects to improve cold-start performance. UTC has every expectation of exceeding the targets at both the single-cell and short stack level, as well as demonstrating these improvements in complete fuel-cell systems.

Criteria	DOE 2010 Target	UTC Internal 2010 Target	UTC Status, 2006
Cold start-up time	30 sec to 50% of rated power from -20 ºC	30 sec to 50% of rated power from -30 ºC	47% rated power in 30 sec from -30 ºC after anode side freeze (single-cell); 34% rated power in 30 sec from -30 ºC after cathode side freeze (single-cell)
Cold start-up time	5 sec to 50% of rated power from +20 ºC	No target	94% rated power in 5 sec from +23 ºC (single-cell)
Unassisted start from low temperature	8 hour soak at -40 ºC	No target	Unassisted start from -35 ºC after 8-hour soak at -35 ºC (short stack)
Survivability	No target	100 cycles to -40 ºC with no performance loss	100 cycles to -40 ºC with no performance loss (short stack)

Table 1. Status of UTC freeze capability.

Conclusions and Future Directions

Excellent BSS and freeze durability results have been achieved with UTC's micro-porous plate PEFCs, which provide water management capabilities unavailable with traditional solid plate PEFC designs. The most important factor in freeze decay appears to be movement of water with thermal gradients, according to the frost-heave mechanism. All results, therefore, are strongly dependent on managing the amount of water present in the cell on shutdown, the movement of water during freeze, and the water production, movement, and removal during start. With this additional mechanism to control water transport under various conditions, UTC's desgin affords more options to manage the cold-start process. For example, UTC has found that no forced reactant purging of the cells is required on shutdown to remove excess water.

UTC's baseline short-stacks performed a successful BSS from -35°C and 100 freeze-thaw cycles to -40°C. No decay was caused by the freeze-thaw cycling, but the freeze/BSS caused some recoverable decay on the anode side of the stack. Ionomer dry-out during freeze and/or cathode flooding during freeze or BSS cause some cells to perform poorly during and after BSS.

Using an MEA with a different catalyst layer structure helped mitigate some of the decay but did not by itself solve the problem. Using GDLs with low liquid permeability, in combination with the modified MEA, largely solved the anode side problem. Preliminary investigations indicate that further GDL permeability optimization may be conducted, offering the prospect of further improvements in performance before and after BSS. A short stack with the new MEAs and GDLs also completed 100 freeze-thaw cycles with negligible performance loss except on the two end-cells. This result complements a separate project (funded by BMW, not DOE) in which a UTC short stack with the new MEAs and GDLs accomplished 200 frozen starts from -10°C with no decay.

Modification of UTC's baseline cell design yielded some improvement, but the most recent results indicate that when combined with the low permeability GDLs, the baseline cell is actually more effective than the lower thermal mass design. This result underlines the success of water-filled micro-porous plates in water management both at operating temperature and below freezing. Using water-filled WTPs to manage water, along with modications to the GDL and MEA, provide a realistic path to meeting and exceeding the DOE and industry-wide freeze targets.

The DOE-funded freeze program was completed on April 30, 2007, but freeze work continues at UTC Power and UTRC. Work at the single-cell, stack, and system is ongoing. Further optimization of cell design and materials is required and is being pursued in order to achieve even faster cold-start times. System simplification continues with the goal of improved robustness.

Cost Status

The DOE cost, the cost share, and the total cost, through April 30th, 2007, are shown in the table below.

	Recipient funded share of outlays	Federally funded share of outlays	Total outlays
Cost through April 30th, 2007	$248K	$990K	$1238K

Summary of cost status for 1st Quarter, 2007

Acknowlegements

Colin Valentine performed many of the single cell cold start experiments. Paul Hunt ran the short stack cold start tests. John Needham designed and fabricated the single cell test hardware. Ryan Balliet helped with organization and execution of the program, as well as analysis of freeze-related phenomena.

FY 2006 Publications/Presentations

1. DOE Annual merit review, poster FCP 21.